University Mohamed Khider of Biskra
Faculty of Fundamental Sciences, Nature and Life Science
Department of Matter Sciences

MASTER DISSERTATION

Matter Sciences
Physics
Energetics and Renewable Energies

Réf. :

Presented and defended by :
Khaoula Abdelli
and
Lynda Abdelli

20-9-2020

Design of Perovskite Solar Cells

Jury :

Mrs	Afak Meftah	Professor	University of Biskra	President
Mr	Nouredine Sengouga	Professor	University of Biskra	Supervisor
Mr	Rami Boumaaraf	Lecturer B	University of Biskra	Examiner

Année universitaire : 2019/2020

Acknowledgment:

We thank god for giving us the will and the courage to achieve this memoir.

We would like to express our sincere thanks to our supervisor for his patience and his precious advices.

We also wish to thank all the friends who have helped from near or far to accomplish this work.

Finally, we want to thank our families for their ongoing support both financially and emotionally.

Abstract:

Perovskite solar cells have become a hot topic in the solar energy device area. With 10 years of development, the energy conversion efficiency has seen a great improvement from 2.2% to more than 22%, and it still has great potential for further enhancement. Numerical simulation is a crucial technique in deeply understanding the operational mechanisms of solar cells and in predicting the maximum value of a solar cell with controlled design. This technique can also give guidance on the structure optimization for different devices.

For the simulations of our PSC model, CuI, CuO, Cu_2O, and CuSCN have been used as the HTM layer. From the simulations, it has been deduced that J-V characteristics of all the PSC models have indicated high-efficiency performance. Among them, the best performance has been achieved for $TiO_2/CH_3NH_3PbI_3/Cu_2O$ PSC structure. Different back contacts were used for simulations to evaluate their effect on the performance of our proposed models. Simulations have been done to analyze the effects of electrical parameters on PSC. A downfall of efficiency has been noticed with the increase of trap density at the $TiO_2/CH_3NH_3PbI_3$ interface layer and also with the increase of perovskite defect density. An increase of efficiency has been observed with the increase of both perovskite and Cu_2O thickness and also with increase of Cu_2O doping concentration. From the results of the simulations, it can be summarized that $TiO_2/CH_3NH_3PbI_3/Cu_2O$ PSC structure is a potential alternative for the third generation solar cell which can be reasonably efficient and inexpensive. Experimental studies are needed for extensive investigation regarding our proposed PSC structure.

Keywords: perovskite solar cells, Scaps-1D, optimization, HTL.

الملخص:

أصبحت خلايا الشمسية البيروفسكايت موضوعًا ساخنًا في مجال أجهزة الطاقة الشمسية. ومع 10 سنوات من التطوير، شهدت كفاءة تحويل الطاقة تحسنًا كبيرًا من 2.2٪ إلى أكثر من 22٪، ولا تزال لديها إمكانات كبيرة لمزيد من التحسين. المحاكاة العددية هي تقنية حاسمة في فهم الآليات التشغيلية للخلايا الشمسية بعمق وفي التنبؤ بالقيمة القصوى لخلية شمسية ذات تصميم متحكم فيه. يمكن أن تقدم هذه التقنية أيضًا إرشادات حول تحسين البنية للأجهزة المختلفة.

لمحاكاة نموذج PSC الخاص بنا، تم استخدام CuI و CuO و Cu_2O و CuSCN كطبقة HTM.و من خلال عمليات المحاكاة، تم استنتاج أن خصائص J-V لجميع نماذج PSC أظهرت أداء عالي الكفاءة. من بينها، تم تحقيق أفضل أداء لبنية PSC ب TiO_2 / $CH_3NH_3PbI_3$ / Cu_2O. تم استخدام وصلات خلفية مختلفة في عمليات المحاكاة لتقييم تأثيرها على أداء النماذج المقترحة لدينا. كما أجريت عمليات محاكاة لتحليل تأثيرات المتغيرات الكهربائية على PSC. لوحظ انخفاض في الكفاءة مع زيادة كثافة العيوب في السطح الفاصل TiO_2 / $CH_3NH_3PbI_3$وأيضًا مع زيادة كثافة العيوب في البيروفسكايت. وقد لوحظت زيادة في الكفاءة مع زيادة كل من سمك البيروفسكايت و Cu_2O وكذلك مع زيادة تركيز تطعيم Cu_2O. و من نتائج عمليات المحاكاة، يمكن تلخيص أن بنية TiO_2 / $CH_3NH_3PbI_3$ / Cu_2O ل PSC هو بديل محتمل للجيل الثالث من الخلايا الشمسية التي يمكن أن تكون فعالة وغير مكلفة. ومع ذلك نحن بحاجة لدراسات تجريبية لإجراء دراسة مكثفة فيما يتعلق بهيكل PSC المقترح.

الكلمات المفتاحية : خلايا بيروفسكايت الشمسية، SCAPS-1D، تحسين، HTL.

Table of contents:

List of figures :

List of tables :

List of common acronyms and symbols:

PSCs – Perovskite solar cells.

ETL – electron transport layer.

HTL – hole transport layer.

DSSC – dye-sensitized solar cells.

PCE – power conversion efficiency.

spiro-MeOTAD – 2,2',7,7'-Tetrakis(N,N-di-p-methoxyphenylamine)-9,9'-spirobifluorene.

PEDOT:PSS – Poly(3,4-ethylenedioxythiophene)-poly(styrenesulfonate)).

PCBM – phenyl-C61-butyric acid methyl ester.

PTAA – Poly[bis(4-phenyl)(2,4,6-trimethylpenyl)amine .

P3HT – poly(3-hexylthiophène-2,5-diyl).

PV – photovoltaic.

HOMO – Highest Occupied Molecular Orbital.

LUMO – Lowest Unoccupied Molecular Orbital.

VB – valence band.

CB – conduction band.

SCAPS – Solar Cell Capacitance Simulator.

Eg – semiconductor's band gap.

χ – electron affinity.

ε – dielectric constant.

Nv and Nc – valence and conduction band density of states.

μ – Mobility.

ND – Donor density.

NA – Acceptor density.

Vth – Thermal velocity.

T – Temperature.

α – absorption constant.

AM – Air mass coefficient.

J-V – Current-voltage.

C-V – Capacitance-voltage.

φ – Potential.

q – Elementary charge.

n – Electron density.

p – Hole density.

Jn – Electron current density.

Jp – Hole current density.

G – Generation rate.

R – Recombination rate.

pt – trapped hole density.

nt – trapped electron density.

Dn – electron diffusion coefficient.

Dp – hole diffusion coefficient.

Ef – Fermi level.

kB – Boltzmann constant.

Ec , Ev – energy levels under a steady state.

D – diffusion constant.

τ – carrier lifetime.

ni – Intrinsic carrier density.

ϕm – work function.

h –Planck's constant.

v – light speed.

Voc – open circuit voltage.

Jsc – short circuit current density.

FF – fill factor.

General introduction:

In recent years, the demand for sustainable and clean energy resources has led to an intense growth in the development of solar cells that directly convert sun light into electricity. Solar cell is one of the most promising technologies for harvesting the sun energy as the largest noncarbon-based natural source. Photovoltaic technology should meet three factors of efficiency, stability, and low cost to reach the industrial demonstration. Silicon photovoltaics as the first generation solar cells are stable, with long lifetime around and high power conversion efficiencies. There are three types of silicon, used in this generation of solar cells: single crystalline silicon (c-Si), multi crystalline silicon and amorphous silicon (a-Si). However, c-Si is expensive and involves high cost of fabrication. This has increased recent research interests into the next generation of thin film solar cells. In an effort to reduce the fabrication costs of the present technology based on Si, and to increase material utilization, thin film materials have been the subject of intensive research. This second generation materials had been developed to reduce production costs of solar cells without jeopardizing their energy output. Three main types of materials have emerged as the most promising candidates for this generation of solar cells. These are hydrogenated amorphous silicon (a-Si:H), cadmium telluride (CdTe) as well as copper indium diselenide (CuInSe2) and its related alloys like Copper Indium Gallium diselenide (CIGS). Although these thin film solar cells have a competitive edge on the first generation solar cells because of lower costs and good efficiencies, they have some drawbacks. Most of the material that these cells are made of are both becoming increasingly rare and more expensive (indium) or are highly toxic (cadmium). To mass-produce these solar cells would also require new facilities, which would greatly increase the cost of production. Because of these drawbacks, a different generation of solar cells has been inspired. This new generation includes Organic/polymer and dye-sensitized solar cells. Organic photovoltaic solar cell (OPV) technology employs semiconducting polymers as low cost materials alternatives to inorganic photoactive semiconductors (silicon, CdTe and CIGS). The third generation of solar cells is the cheapest of all the other solar cell generations. The efficiency of organic solar cell generation is generally very low.

With the relentless effort of researchers in photovoltaics, perovskite solar cells (PSCs) have recently emerged as one of the possible ways to have a low cost and highly efficient solar cell. The

light harvester layer in these solar cells are perovskites which are solution processable materials and also show properties of optoelectronic materials studied in solid state physics. This type of unpredictable coalescence has led the solar photovoltaic to be processable at room temperature and compatible to Si-based solar cells. PSCs are good but there are some challenges like lifetime, instability caused by heat and moisture and lack of uniformity on which a lot of work has to be done. The PCE of PSCs depends on the physical parameters of the materials which we are using as light harvester (perovskites), electron transport layer (ETL), hole transport layer (HTL), contacts and also on the device structure.

In order to improve the performance of a photovoltaic solar cell, it is necessary to optimize it by simulation, because it follows a mathematical model of the real system, it has the advantage of being easy, inexpensive, and we can predict the optimal parameters that contribute to making a cell with the best performance. The objective of this work is to model the effect of parameter layers on the electrical characteristics (short circuit current density Isc, open circuit voltage Voc, Form factor FF, The conversion efficiency of the solar cell studied η) of a Perovskite-based solar cell in order to optimize it by simulation using SCAPS-1D software.

This dissertation is organized as follows:

The first chapter presents the history of PSCs, there working principle, the material perovskite, ETL and HTL materials and there properties.

The second chapter is Presentation of the simulation software SCAPS-1D and the Cu-based materials and there properties.

In the last chapter we present and discuss the results obtained.

Chapter I: perovskite solar cells

Chapter I: perovskite solar cells

I.1 Introduction:

In an effort to develop cost-effective photovoltaic systems alternatives to silicon solar cells, perovskite-based solar cells have attracted considerable interest. the efficiency of perovskite solar cells has increased to high levels, surpassing the efficiencies of many commercial photovoltaics, such as dye-sensitized, organic and amorphous silicon solar cells. In this chapter, firstly we explained the development of PSCs, there structure and there working principal. Secondly, we talked about properties of the absorber layer (material, structural and optoelectronic properties). Then we described the different transport materials and there properties as ETLs and HTLs.

I.2 Perovskite solar cells:

I.1.1 History of perovskite solar cells:

The base technology for perovskite solar cells (PSCs) is solid-state sensitized solar cells that are based on dye-sensitized Gratzel solar cells [1] . In 1991, inspired by the principle of photosynthesis, O'Regan and Gratzel reported a landmark construction of solar cell called dye-sensitized solar cell (DSSC), which can convert the sun light energy into electricity with an efficiency of about 7% [2]. Presenting numerous advantages such as abundant raw materials, facile processing, and low cost compared with conventional solar cells, these novel solar cells made itself investigated popularly rapidly after its arising, and it is this work that inspired the emergence of PSCs, a DSSC with perovskite compounds [3]. The general chemical formula of perovskite compound is ABX_3 which is similar to that of calcium titanium oxide ($CaTiO_3$), revealed by the German mineralogist Gustav Rose in the year 1839. The structure was afterwards described by Russian mineralogist Lev. Perovski, from where it gets its name [4].

The first perovskite solar cell (PSCs) was reported by Kojima and co-workers in 2009 [5]. They used methylammonium lead iodide ($CH_3NH_3PbI_3$, 'MAPbI$_3$') and methylammonium lead bromide ($CH_3NH_3PbBr_3$, 'MAPbBr$_3$') as solid sensitizers in dye-sensitized solar cells (DSSCs) with liquid electrolyte. Due to dissolving of perovskite in liquid electrolyte , these DSSCs with short lifetime

(a few minutes) showed a low power conversion efficiency (PCE) of 3.13% and 3.81% for $MAPbI_3$ and $MAPbBr_3$ solar cells, respectively. The work did not gain much attention due to low efficiency and poor stability, which resulted from a hole transport layer (HTL) with liquid electrolyte [3]. Two years later, the PCE of the perovskite-sensitized photocells reached 6.5% by optimizing the thickness of photo anode and modifying interfaces [6] through the TiO_2 surface treatment in 2011. In 2012, Park and Grätzel et al. first introduced the solid-state hole transporting material (HTM), spiro-OMeTAD, into the perovskite solar cell to replace the liquid electrolyte and an impressively high efficiency of 9.7% [7] was obtained. In the same year, Snaith and colleagues reported perovskite solar cells using Spiro-MeOTAD based HTM and Al2O3 as scaffold. The device presented an efficiency of 10.9%. In their report, they showed that a better performance can be obtained by using mixed-halide ($CH_3NH_3PbI_{3-X}Cl_3$) due to improved ability of charge transport. They also showed that perovskites had a bipolar charge carrier transport of electron and hole [8]. In 2013, Seok, Grätzel and colleagues reported an efficiency of 12.3% by using the structure of nanoporous TiO_2 infiltrated by mixed-halide perovskite [9]. Simultaneously, an efficiency over 15% was reported from Burschka and group members by using TiO_2 scaffold and iodide deposition [10]. Snaith removed scaffolding from the device and applied planar structure, obtaining similar conversion efficiency compared with the report by Burschka et al [11]. Subsequently, efficiencies of 16.2% and 17.9% were reported by Seok et al. in early 2014 by using $CH_3NH_3PbI_{3-X}Cl_X$ and a poly-triarylamine HTM [12-13]. In 2016, Saliba introduced a perovskite solar cell with an efficiency of 21.1% by using a mixture of triple cation (Cs/MA/FA). It showed high stability and reproducibility [14]. Seok and co-workers introduced an approach to reduce defects in the perovskite layer by using an intramolecular exchanging process in 2017, which is favorable in reducing the defects concentration, and they obtained an efficiency of over 22% [15].

The significant improvement in the performance of perovskite solar cells within 8 years is short, and the efficiencies were enhanced rapidly from 3.8% to about 22%. It is expected that the efficiency can be further improved with efforts. However, behind the high efficiency, more physical and chemical investigations into this cell are still needed for a better understanding of the impressive success.

I.1.2 Structure of perovskite solar cells:

To date, two main architectures of perovskite solar cells are studied, the mesoporous and the planar. Figure.1.1 shows evolution of device configuration in perovskite solar cells. Perovskite was first used as a sensitizer in DSSCs (Figure.1.1(a)) [16]. In this case, the $MAPbI_3$ nanocrystals were deposited on the mesoporous TiO_2 (mp-TiO_2) instead of dye [17], HTM (Hole Transporter Material) is infiltrated into the layer of mesoporous oxide (TiO_2). The compact layer is made of the same material as the mesoporous layer, a transparent conductive material, titanium oxide (TiO_2). Having the properties of an electron collector, TiO_2 is used to separate the charges generated in the perovskite [16]. The drawback of this design consists mainly in the high temperature usually required for producing an effective TiO_2 layer, but other low temperature techniques applicable to flexible substrates have been developed [18].

In one study, the mesoporous scaffold may be composed of Al_2O_3 nanoparticles where, the TiO_2 nanoparticles were replaced by Al_2O_3 nanoparticles (Figure I.1(b)). The performance of cells [19] has shown that they can function in the absence of the mesoporous TiO_2 layer. This kind of approach has been investigated especially in cells in combination with $CH_3NH_3PbI_{3-X}Cl_X$ perovskite with which better results have been produced. The Al_2O_3 layer only acts as a support for the photoactive layer. However, the scaffold definitely modifies the substrate enabling an easier growth of a homogenous perovskite layer, even without a high temperature-sintering step [20]. Indeed, because of the energy levels of the conduction bands of these two materials, the injection of perovskite towards this layer is impossible. In this case, the transfer of electrons takes place directly between the perovskite and the compact TiO_2 without injection into the nanoparticles. This highlights the transport of charges in the perovskite [21].

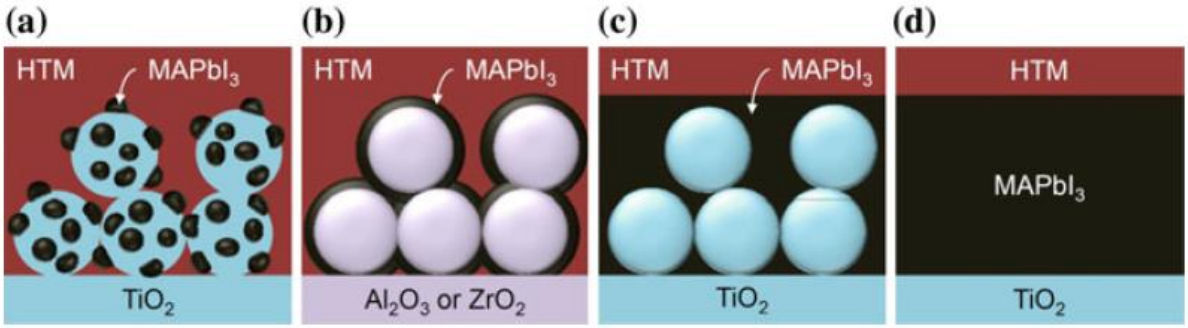

Fig I.1 Evolution of device configuration in perovskite solar cells. (a) sensitization concept, (b) extremely thin layer of perovskite deposited on mesoporous scaffold layer, (c) perovskite infiltration into mesoporous film and (d) planar heterojunction structure[21].

A mesoporous block structure (Figure.1.1(c)) was then proposed in which the perovskite covers the surface of the TiO2 nanoparticles after filling the pores of the mesoporous film. After infiltration with perovskite, a compact and thick layer is formed on top of the oxide layer. The perovskite can also be directly deposited between a TCO and an HTM planes in order to create PSCs with plane heterojunction, that is to say an architecture of the type "thin layers" (Figure I.1(d)) [16].

The mesoscopic structure can be divided into regular (n-i-p) and inverted (p-i-n) structure depending on which selective contact is used on the bottom (Fig I.1 a, b). The regular n-i-p structure has been extensively studied and was based on dye-sensitized solar cells.
The conventional n-i-p mesoscopic structure was the first arrangement of perovskite photovoltaics to be tested [22]; the assembly begins with a transparent glass cathode followed by the electron transportation material (ETM). The structure is then layered with a mesoporous metal oxide containing the perovskite, followed by the hole transport material (HTM), and capped with a metallic anode (Fig I.2(a)). This initial advancement in PSCs created an important field of interest for photovoltaic researchers and consequently led to the development of other PSC device configurations (Fig I.2(c, d)).

The planar architecture is an evolution of the mesoscopic structure, where the perovskite light harvesting layer is sandwiched between the ETM and HTM. The absence of a mesoporous metal oxide layer leads to an overall simpler structure. It is possible to achieve a high efficiency without the mesoporous layer by carefully controlling the interfaces between the different layers that make up the PSC (the perovskite light absorber layer, the electron transporting layer, the hole-transporting layer, the electrodes as well as the perovskite layer itself) [23]. With the same materials and approach, a planar n-i-p PSC shows increased V_{OC} (open-circuit voltage) and J_{SC} (short-circuit current density) relative to a mesoscopic PSC device. Efforts have been put in optimizing the interfaces at the contacts to improve electron injection [23]. For instance TiO_2 can be substituted with ZnO [24] or SnO_2 which offer much higher electron mobility [25], obtaining better

performance and reduced hysteresis; however, the planar configuration also had more severe J-V hysteresis which calls into question the accuracy of the reported efficiencies [26]. The grain and thickness of this buffer layer influence the J-V hysteresis behavior [27]. Kim et al. also observed that J-V hysteresis problem is significantly dependent on the P-type hole-transporting materials and found that the hysteresis behavior can become negligible with a reduced capacitance, which can be done by replacing Spiro-OMeTAD with poly (3,4-ethylene dioxythiophene)-poly(styrene sulfonate) (PEDOT:PSS) or any other inorganic hole-transporting materials[28]. However, the J-V hysteresis behavior is also dependent on voltage scan direction, scan rate, and range. To counter this problem, a thin mesoporous buffer layer was incorporated within the planar n-i-p PSC structure [29].To date, the best mesoscopic n-i-p device has exhibited a PCE 21.6 % [30], whereas the highest reported efficiency of a planar n-i-p cell 20.7 % [31]. Although mesoporous PSC shows better efficiency than planar structure, it is required to have a thinner mesoporous layer (less than 300 nm)[32]. In addition, the planar device could be fabricated with a low-temperature process unlike the mesoporous structure. However, better control of the perovskite-absorbing layer is required [33].

The first inverted planar structure of perovskite solar cells adopted a similar device structure to the organic solar cell [34]. In the case of the p-i-n planar perovskite architecture, the HTM layer is deposited first followed by the ETM layer. It was discovered that perovskites are capable of transporting the holes themselves , which led to Jeng et al. developing the first planar hetero-junction PSC with an inverted structural design [35]. With this advancement, the inverted p-i-n configuration has expanded the options to explore more for selective layer from organic to inorganic materials and the use of oxide HTM allow for constructing mesoscopic p-i-n device architecture [36]. Planar p-i-n PSC offers low-temperature processing, negligible hysteresis behavior with high efficiency of 18% [37]. The device configuration of the inverted p-i-n planar and mesoscopic PSC is shown in Fig I.2(c, d).

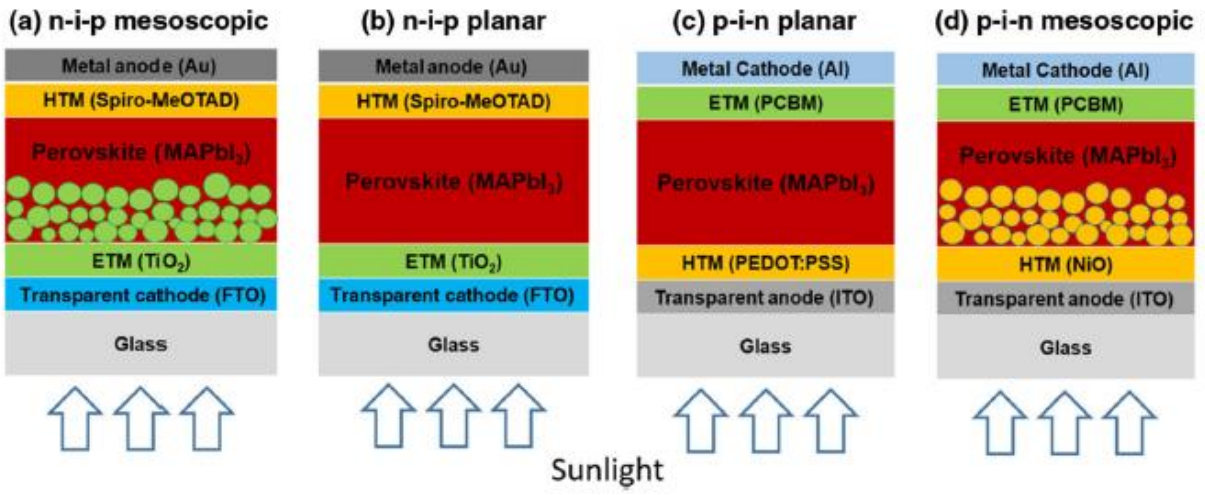

Fig I.2 Schematic showing the layered structure four typical of perovskite solar cells: (a) n-i-p mesoscopic, (b) n-i-p planar, (c) p-i-n planar, and (d) p-i-n mesoscopic [28].

At present, PSCs in mesostructured architecture are more efficient than those with plane heterojunction due to better charge transport and a decrease in recombination. However, for a perovskite with a longer diffusion length, a plane junction would then be favorable for efficient collection and transport of charges without significant recombination [38].

I.1.3 Working Principles of Perovskite Solar Cells:

In a PSC, the perovskite layer is sandwiched between a p-type layer, also called HTM (Hole Transport Material), and a n-type layer, also called ETL (Electron Transport Layer), creating a p-i-n configuration. The success of perovskite as a solar absorber is largely dependent on the long charge diffusion length and high carrier mobilities in the medium. The electron and hole diffusion length in perovskite medium can reach as high as 1 μm which is large enough for the photo-generated charges to reach the interfacial layers and electrodes without geminate and non-geminate recombination, depending on the morphology of the perovskite medium [39]. The carrier mobilities are reported to be as high as 25 $cm^2/(Vs)$ [40] which is three order of magnitude greater than the mobilities in bulk heterojunction organic solar cells. There two main device architectures known today in the preparation of perovskite solar cell are mesoporous-PSC and planar-PSC structures. Hence, the charge transport channels in PSC are often discussed in terms of the nature of these two device structures (figure I.3).

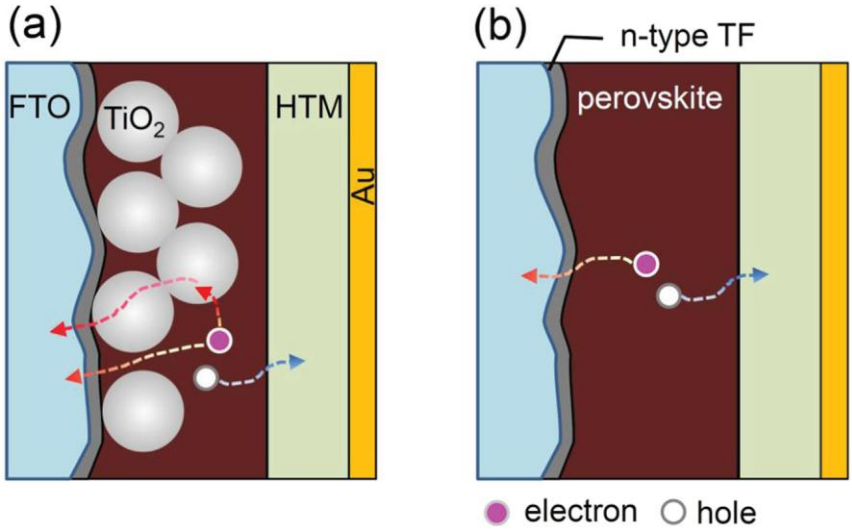

Fig I.3 Charge transport channels in perovskite solar cells (a) using mesoporous medium (b) planar perovskite structure[41].

In mesoporous structure, light is absorbed by the perovskite material, which leads to excitation of an electron from valence to conduction band of perovskite and the creation of an electron-hole pair (fig I.4(a)). The charges dissociate readily thanks to the low exciton binding energy and they are free to move across the device. Electrons can either diffuse through perovskite to the mesoporous scaffold (if present and made out of suitable electron transport material such as TiO2). Subsequently, electrons are collected at the electrode (figure I.4(b)). Photogenerated holes diffuse through perovskite to reach HTL, from where they are collected at the metal electrode[42].

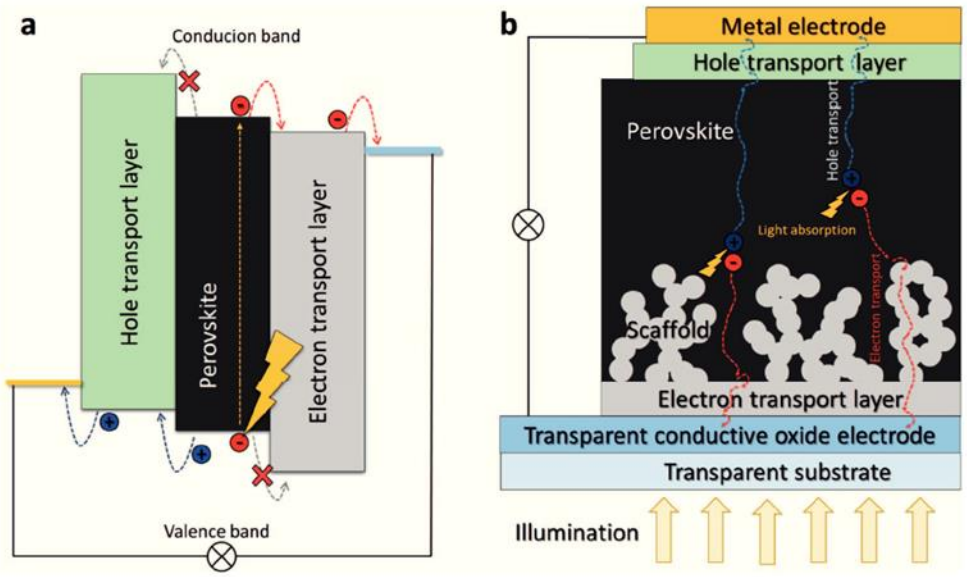

Fig I.4 Working principles of PSCs with (a) the schematic energy diagram of a PSC. (b) Schematics of the "normal" architecture PSC with mesoporous scaffold. Charge generation and transport processes are presented schematically[43].

In the case of planar structure, the devices are fabricated using interfacial buffer layers of hole and electron transport material (ETM and HTM) through which the photo-generated charges created in the photoactive medium can be driven to the electrodes by the influence of either built in potential or external applied field.

Electron and hole transport layers (also referred to as "blocking" or "charge selective" layers) are vital parts of PSCs. Their main role is to prevent the "wrong" charges being collected at the electrodes, while allowing the "right" ones to pass. This is achieved by the selection of materials with appropriate energy levels with respect to those of perovskite. An example of the set of materials used as ETLs and HTLs is shown in Fig I.5.

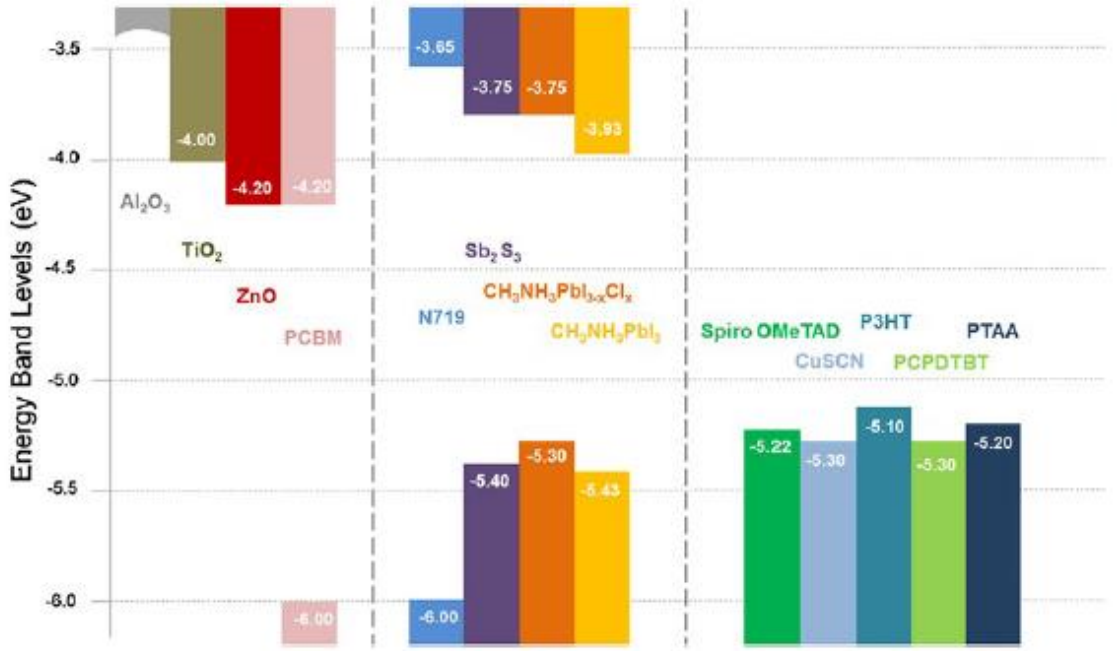

Fig I.5 Energy levels for different materials acting as ETLs (left), absorbers (middle) and HTMs (right) in perovskite solar cells[42].

A good HTL materials should have its conduction band or lowest unoccupied molecular orbital (LUMO) far above that of the perovskite . At the same time, its valence band or highest occupied molecular orbital (HOMO) should be just slightly above the perovskite valence band. The opposite is required for ESL material as depicted Figure I.5. Lack of this charge selectivity is very detrimental to the device. If, for example, an electron reaches the metal contact, it recombines non-radiative with one of many holes present at the contact [44]. This process leads to loss of photo-generated charges and hence it is highly unwanted.

Charge recombination can additionally occur at defects in the perovskite. This can be at interfaces, grain boundaries or impurities in the perovskite [45]. Again, this results in non-radiative.

I.3 Perovskite material:

Perovskite is a mineral with the chemical formula $CaTiO_3$[46], perovskite has an ABX_3 crystal structure, the cation A occupies the eight vertices of a cube surrounded by twelve anions X, while

the cation B is in the center of an octahedron formed by six anions X $[BX_6]^{4-}$ located at the centers of the faces of the cube [47]. The crystal structure of perovskites is illustrated in Figure 1. Perovskites are divided into two groups; perovskites in the form of oxides which are inorganic and halogenated perovskites which may be inorganic or hybrids (inorganic-organic) [48]. In the case of oxides, X represents an oxygen atom O, B is a tetravalent metal cation such as Ti^{4+} , Si^{4+} and Sn^{4+},…, and A represents a divalent cation such as Mg^{2+}, Ca^{2+}, Sr^{2+}, Ba^{2+}, ... In the case of halogenated perovskites, X is a halogen atom, Cl^-, Br^- or I^- , B represents a divalent ionic metal such as Pb^{2+} or Sn^{2+}. Element A can represent a monovalent alkali metal such as Li^+, Na^+, K^+, Rb^+ or Cs^+ (case of an inorganic halogenated perovskite) or a small organic molecule such as methylammonium ($CH_3NH_3I^+$=MA) or formamidinium ($HC[NH_2]^{2+}$=FA) (case of hybrid materials) [49, 50]. The replacement of A by the MA cation to generate the first three-dimensional hybrid perovskites has been published by Weber et al [51].

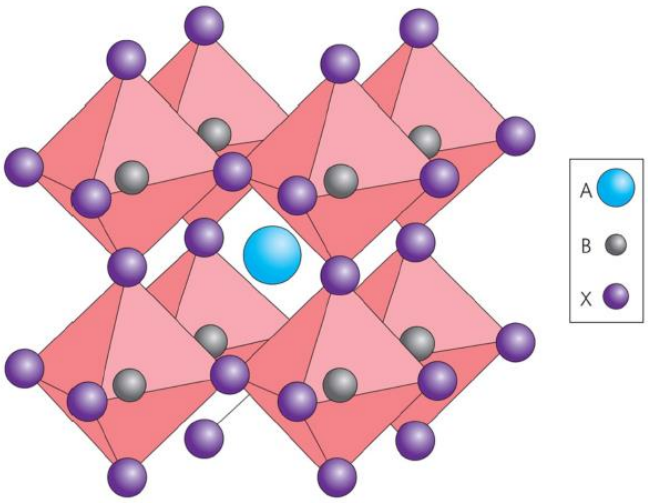

Fig I.6 the Perovskite crystal structure [12].

Halogenated hybrid perovskites have attracted the most attention in the photovoltaic field in recent years given the chemical, and therefore, structural diversity of perovskite materials. Their physical properties are distinct and have found a broad range of applications in material science. Perovskites have become prominent in the fields of ferroelectrics, superconductors and more recently in photovoltaics [52].

The solar cells based on organometallic halide perovskite $CH_3NH_3PbI_3$($MAPbI_3$) have had a remarkable increase in the photoelectric conversion efficiency [53]. Because the organometallic perovskite materials have a series of magical properties, such as strong optical absorption coefficients, low carrier recombination rates, and ease of fabrication, which has been successfully employed in different kinds of solar cells such as mesoporous structures and planer structures [54]. Consequently, $CH_3NH_3PbI_3$ material has become star materials in the photovoltaic field [55], and the basic properties of perovskite $CH_3NH_3PbI_3$ such as the electronic structure, the microscopic mechanism of charge balance transport [56], in addition to the widely used $CH_3NH_3PbI_3$, the chlorine-incorporated perovskite,$CH_3NH_3PbI_{3-X}Cl_X$, is also attracting increasing attentions. As for the planar structure perovskite solar cell, $CH_3NH_3PbI_{3-X}Cl_X$-based device could reach a PCE as high as 19.3%, which is much higher than the $CH_3NH_3PbI_3$-based one [57].

The instability of perovskite at high relative humidity is one issue that needs to be addressed. One method used to solve this problem is the creation of a mixed halide perovskite. The simple solution mixture of $CH_3NH_3PbI_3$ and $CH_3NH_3PbBr_3$ was reported to result in a solid solution of $CH_3NH_3PbI_{3-X}Br_X$ (x = 0–3) [58].

Maintaining the thermal stability of perovskite materials is critical during long-term applications. The thermal stabilities of $CH_3NH_3PbI_3$ ($MAPbI_3$) have been investigated in different environments from the perspectives of film morphology, chemical composition, and electrical conductivity [59]. The results revealed that $CH_3NH_3PbI_3$ is not intrinsically stable when heated to 85 °C under full sunlight for 24 h, and that $CH_3NH_3PbI_3$ in devices breaks down not only in air but also under nitrogen gas. The poor stability of $CH_3NH_3PbI_3$ severely limits its commercialization application. Another widely used perovskite material is $CH(NH_2)_2PbI_3$($FAPbI_3$). Owing to the reduction of symmetry, the band gap of $FAPbI_3$ was estimated to be 1.48 eV, whereas that of $MAPbI_3$ was 1.52 eV [60]. Under the same test conditions, $MAPbI_3$ and $FAPbI_3$ were used as light-absorbing layers in the device. The $FAPbI_3$- based device exhibited a more excellent PCE than the $MAPbI_3$ - based device [61], demonstrating that $FAPbI_3$ had superior stability over $MAPbI_3$. Researchers have conducted tests to confirm how replacing a MA cation with a FA cation affected the thermal stability [62,63]. The result showed that $FAPbI_3$ was fully stable without decomposition at 150 °C in air, whereas $MAPbI_3$ broke down into PbI_3 and CH_3NH_3, indicating that $FAPbI_3$ has a higher thermal stability than $MAPbI_3$. In addition, thermo gravimetric analysis revealed that the thermal

decomposition temperature of FA-based perovskite (50 °C) was higher than that of MA-based perovskite [62]. This information is helpful for improving the thermal stability of PSCs when FA cations are applied. However, an obvious drawback is the phase stability of the perovskite structure. At room temperature, $FAPbI_3$ tended to form a non-photoactive phase in addition to the photoactive perovskite phase [63].

I.4 Properties of perovskite :

I.4.1 Structural properties :

In order to maintain high-symmetry cubic structure ,the tolerance factor should be close to 1. t is written as : $t = \frac{(R_A+R_X)}{[\sqrt{2}\,R_A+R_X]}$

Where R_A , R_B , R_X are the ionic radii of A,B and X site ions respectively [64]

The perovskite structure is stable when : $0.89 \leq t \leq 01$ .Ideal cubic structure only observed at room temperature when t is close to1.In order to satisfy the ideal tolerance factor ,the A site ion must be much larger than the B site ion. If A ions are small , t < 1and tetragonal , orthorhombic and rhombohedral deformation of structure are caused due to rotation movement[65]

Values of t for compositions:$MAPbI_3$, $MAPbCl_3$, $MAPbBr_3$ are 0.83 ,0.84 ,0.85 respectively , the cubic phase is not stable in atmospheric conditions for these compositions , tetragonal and orthorhombic structure are favorized [66].

In case of hybrid halide perovskite for photovoltaic applications the cation A is the larger element and is generally taken to be methylammonium ($CH_3NH_3^+$) with R_A=0.18nm .The formamidinium($NH_2CHNH_2^+$) with R_A=0.19-0.22nm is another organic cation which provided good results .The anion X is usually taken iodide (I) having radius of 0.22nm ,the bromine (Br) and chlorine (Cl) are also used .The cation B is generally lead (Pb) with $R_B = 0.119nm$[67].

Besides the tolerance factor the stability of the perovskite is also determined by the octahedral factor μ which is used to predict the formation of perovskite structure.μ can be described by :

$\mu = \frac{R_B}{R_X}$ and should lie between 0.44nm and 0.9nm for stable perovskite structure [68] .

Generally ,the ABX_3 perovskite structure can be formed under the conditions of : $0.813< t <1.107$ and $0.442< \mu <0.895$ [69]. Figure 1.7 shows the tolerance factor for some perovskite materials.

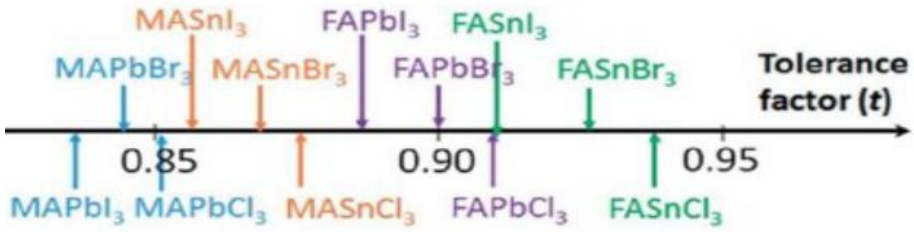

Figure I.7 tolerance factor for different perovskite material systems[70].

Additionally ,the perovskite materials undergo several phase transitions as a function of changing temperature due to a rotation movement of the organic cation.

Transition temperature values depend of the different elements of perovskite material. When temperature is lower than 100 K, the perovskite displayed a stable orthorhombic (γ) phase .With temperature increased to 160 K, the tetragonal (β) phase started to appear and replace the original orthorhombic (γ) phase. As temperature increases further to about 330 K, the tetragonal (β) phase started being replaced by another stable cubic (α) phase[71] .

Figure I.8 displays those three transitions . At high temperatures, $CH_3NH_3PbI_3$ shows a pseudo-cubical α-phase .If the temperature is cooled , the perovskite undergoes a phase transition to the tetragonal β phase. In both α and β the orientation of methylammonium cations is not defined, If the temperature is lower , the perovskite displays an orthorhombic γ phase .

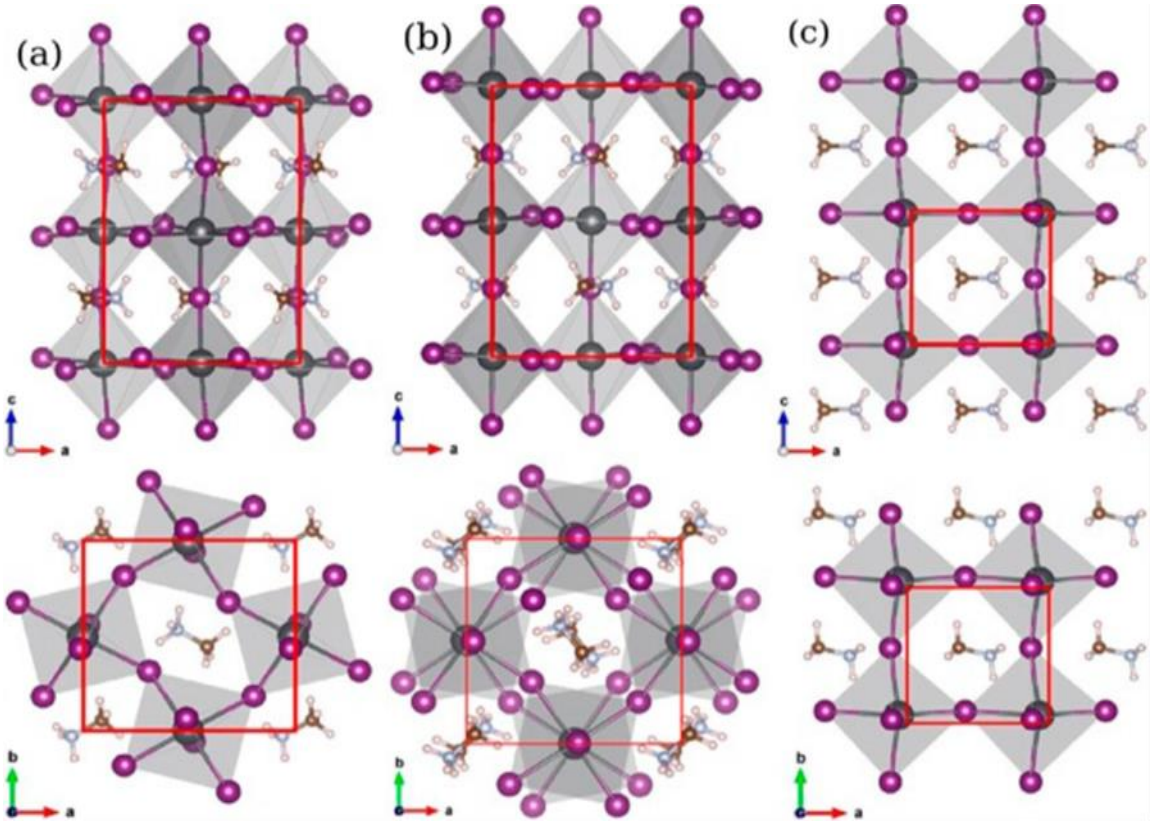

Figure I.8 Comparison of (a) orthorhombic, (b) tetragonal and (c) cubic perovskite phases obtained from structural optimization of $MAPbI_3$.[72]

I.4.2 Optoelectronic properties :

In the hybrid perovskite structure of MAPbI3, the iodine ions at the X-site forms the valence band and the lead (anion) at the B-site forms the conduction band, while organic cation at the A-site remains electronically inactive but contributes to the structural stability and tolerance factor of the perovskite structure. The valence band (or highest occupied molecular orbital, HOMO) is determined by the Pb 6s–I 5p σ-antibonding orbital. Similarly, the conduction band (or lowest unoccupied molecular orbital, LUMO) is determined by the Pb 6p–I 5p π-antibonding and Pb 6p–I 5s σ-antibonding orbitals (Figure I.9) [73].

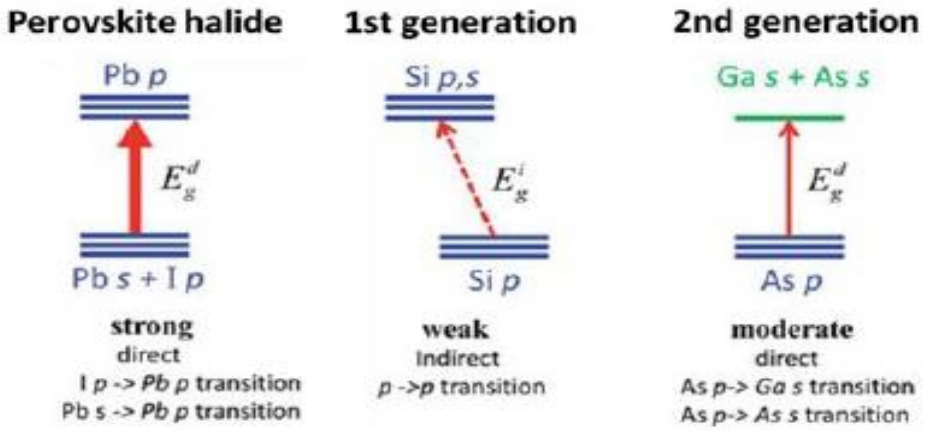

Figure I.9 The schematic optical absorption of: (a) halide perovskite solar cell absorber; (b) first-generation (Si); and (c) second-generation (GaAs as example)[74].

Depending on the halide content ,the bandgap of mixed halide perovskites can be tuned from~1.6eV (pure $MAPbI_3$) to 3.2eV (pure $MAPbCl_3$) (figure I.10). Smaller band gaps can be achieved using appropriate organic cations and inorganic cations [75]. The $CH_3NH_3PbI_3$ perovskites are direct bandgap semiconductors with a value estimated by 1.55eV [76].

Therefore ,hybrid perovskites have very high absorption , thereby greatly reducing the thickness necessary for absorption and collecting efficiently the charge carriers. Absorption in the visible spectrum range is possible with a thickness of 500nm of perovskite film , which is much less than that required in thin film solar cells[34] .

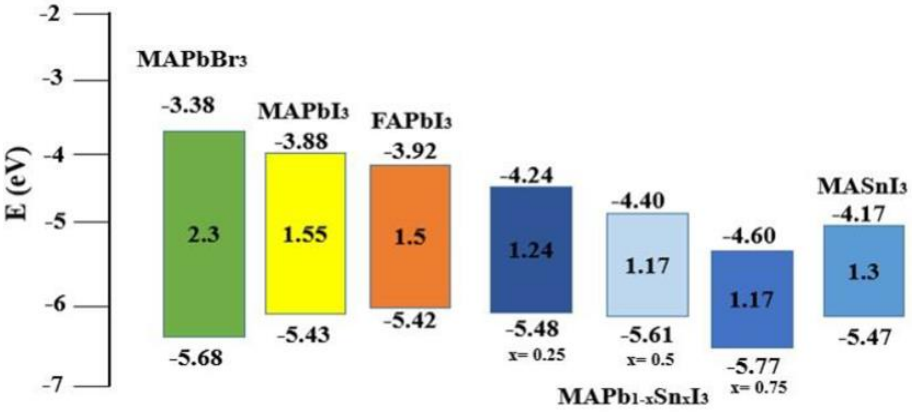

Figure I.10 Schematic illustration of energy level diagram by using different combinations of perovskite Materials.[76]

The absorption onset is close to 800nm with strong absorption in the whole of the visible spectrum. The absorption coefficient of perovskite reaches $10^5 cm^{-1}$ which is much greater than that of crystalline silicon [77].

Perovskite materials displays high and balanced diffusion lengths for both electrons and holes (0.1-1µm) and sufficiently high charge mobilities. This means that the charges can efficiently diffuse to electrodes before recombining. The longest diffusion length (exceeding 3 mm) was observed in a $CH3NH_3PbI_3$ single-crystal under weak light illumination, where a hole diffusion length of ~175µm was measured under one sun illumination (electron and hole mobilities calculated using Hall effect measurements were 105±35 and 24.8±4.1 $cm^2V^{-1}s^{-1}$ respectively)[78].

Additionally , halide perovskites are characterized by low exciton binding energy (30 mV),which means that photo generated charges can separate readily at room temperature .

For recombination ,the effect of such crystal defects and trap levels is not so critical on the device performance . This might explain how PSC can exhibit a very high open circuit voltage of up to 1.1V or more , with a very small voltage loss[79].

I.5 Transport materials :

The efficiency and stability of PSCs depend strongly on the morphology and type of materials selected as ETL and HTL in the device .

I.5.1 Electron transport materials :

In order to achieve high performance PSC the presence of ETL is required to facilitate efficient electron collection and transportation from perovskite to its respective electrodes. Juarez-Perez et al compared the device performance of complete PSCs with ETL-free device and they observed that the absence of ETL has minor impact on the open -circuit voltage (V_{oc}) but severely reduce short circuit voltage (J_{sc}) as well as fill factor (FF) which subsequently affected the PCE of the devices .The insertion of ETL substantially increased the electron-hole recombination resistance (R_{rec}) at the expense of small increment in series resistance (R_s)[80] .

In order to fabricate PSCs with high efficiency ,the materials selected as an ETL must fulfil several criteria .The ETL must possess :

1-good electron mobility to enable fast electron transport within ETL .

2-zide band gap to ensure high transparency and allows more light to pass through it so that light absorption by perovskite materials can be maximized .

3-compatible energy levels where ETL must have compatible conduction band maximum (CBM) and valance band maximum in relative to energy levels of perovskite light harvester to facilitate electrons transfer and block holes transport .

I.5.1.1 Inorganic electron transport materials :

Inorganic materials are used in perovskite solar cells as electron transport materials widely. With high electron mobility, they can effectively carry out the transmission of electrons. The nature of the material determines their strengths and weaknesses[81].

TiO_2 was used as mainly electron transport materials. It can improve the separation and transmission efficiency of excitons due to the good energy level matching between TiO_2 and perovskite materials[82].

In addition ZnO as a metal oxide with high electron mobility is often used as electron transport material in perovskite solar cells. The ZnO is considered as an ideal metal oxide semiconductor for its wide band gap (3.37 eV), a larger exciton binding energy (~60 meV) and the unique characteristics of photoelectric[83].

WO_3 has good stability and resistance to acid corrosion and has a higher mobility than TiO_2; WO_3 was used as the electron transport material in perovskite solar cells. But carriers in the interface of WO_3 and perovskite absorption layer are prone to compound and will reduce the short-circuit photocurrent density of the devices[84].

SnO_2 has a lower conduction band edge, in theory; it is easier to let the electron from light absorption material into the conduction band of SnO_2 . the devices with SnO_2-based electron selective contact have a better stability than TiO_2-based perovskite solar cells[85].

I.5.1.2 Organic small molecule electron transport materials :

Organic small molecular materials have also been used to fabricate electron transport layer. They are easy to be processed and chemically modified to meet different requirements . Common organic small molecule electron transport materials include fullerene and its derivatives.

Wu et al. used chemical bath (CB) solution of PC_{71} BM in the process of making solar cells by the method of spin coating .PCBM can adjust C_{71} energy levels and improve the photoelectric conversion efficiency. Open circuit photovoltage and fill factor of the device are increased obviously[86]. Jeng et al. used organic small molecular material fullerene C_{60} as electron transport material . In their experiments, PCBM and ICBA were also put instead of fullerene C_{60} to make electron transport layer[87].

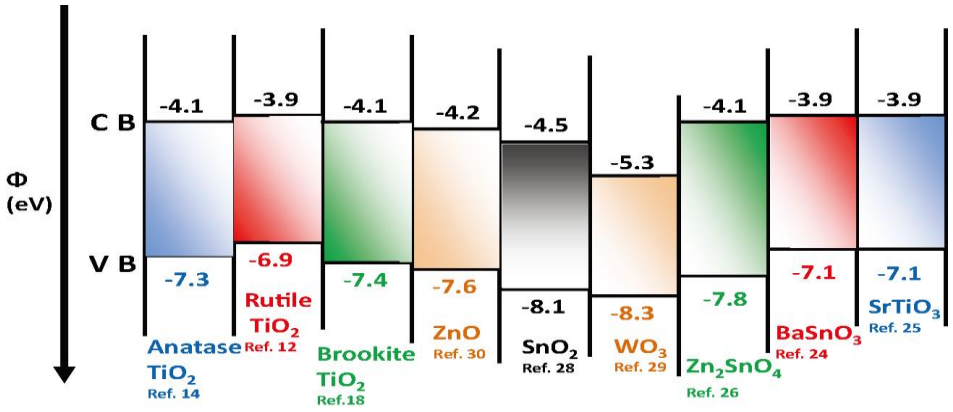

Figure I.11 Schematic diagram illustrating the energy levels of CB and valence band (VB) of n-type metal-oxide electron transport materials[88].

I.5.2 Hole transport materials :

The devices with HTL exhibit substantial increase in power conversion efficiency, open circuit voltage and short circuit current compared to the device without HTL**.** additionally HTL can decrease the recombination around the electrode .

The essential requirements for HTMs in PSCs are :

1-Valence band(VB) of HTM is compatible with the VB of the organic-inorganic halide perovskite.

2- Good hole mobility as it helps to reduce the series resistance and enhance the fill factor (FF).

3-Optical absorption lies in the range of visible to IR range (to minimize optical losses in photovoltaic devices).

4-Excellent thermal and photochemical stability.

5-The thickness of the HTM layer should be maintained to avoid resistive losses and cover the entire perovskite layer to allow better crystalline growth of the perovskite.

Solid state hole carriers can be divided into two categories: organic molecules and inorganic molecules.

I.5.2.1 Organic hole transport materials :

Generally, organic material include long polymer-based HTLs and small molecule-based HTLs, are used as HTM in perovskite solar cells [89]. Spiro-OMeTAD, PEDOT:PPS, PTAA, P3HT ,are the most crosslinked polymers used and other derivatives of smaller molecules like pyrene [$C_{16}H_{10}$] ,thiophene [C_4H_4S] ,porphyrin [$C_{34}H_{34}N_4O$] and carbazole [$C_{12}H_9N$] derivatives [90].

The prominent one used is 2,2',7,7'-tetrakis(N,Ndi-p-methoxyphenyl-amine)9,9'-spirobifluorene (spiro-OMeTAD,$C_{73}H_{52}N_4$). However, due to the limited conductivity of pure spiro-OMeTAD ,oxygen exposure is necessary for high performance devices . In order to expedite the oxidative reaction between spiro-OMeTAD and O_2, (Li-TFSI) is needed as a counterion [90]. (TBP) is another additive added into spiro-OMeTAD to improve the open-circuit voltage. However, TBP and acetonitrile which are the solvent to dissolve Li-TFSI, could degrade perovskite [91].

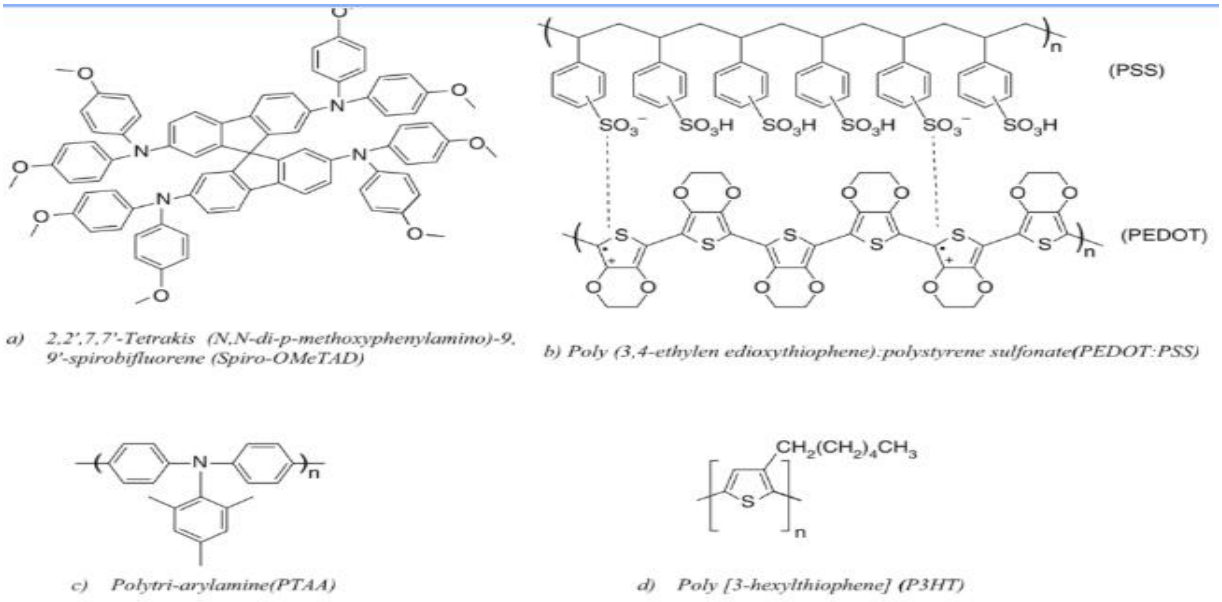

Figure I.12 molecular structure of organic HTLs.[92]

organic hole-transporting materials (HTM) used are normally quite expensive due to complicated synthesis procedures or high purity requirements. Moreover, the instability of these organic compounds has been a major issue with regard to commercial applications[93].

I.5.2.2 Inorganic hole transport materials :

Inorganic materials are considered as promising materials for the HTM layer because of their favorable characteristics, such as high mobility of hole, low cost of fabrication, better chemical stability, and appropriate valance band position.

CuSCN, CuI, Cu_2O, CuO, NiO, MoOx ,CZTS and carbon materials (including graphene and carbon nanotube (CNT)) are used as inorganic HTM in perovskite solar cells [93].

Among the proposed materials Copper thiocyanate (CuSCN) forms the appropriate one. the good alignment between the HOMO level of the CuSCN and of the $CH_3NH_3PbI_3$,also the mobility which plays a crucial role between materials that have almost similar band alignment proprieties [94].

Kesterite-structured Cu_2ZnSnS_4 (CZTS) nanoparticles exhibits low bandgap (1.5 eV), high hole mobility (6-30 $cm^2V^{-1}s^{-1}$), high absorption coefficient and earth abundant elemental constituents [95]. Thus, this material acts as inorganic HTM for organo-lead halide PSCs.

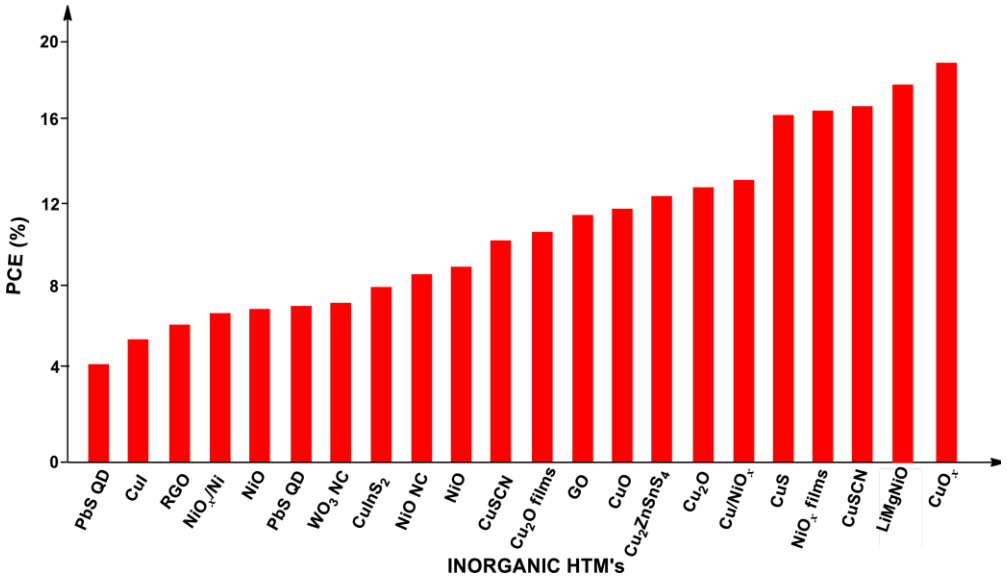

Figure I.13 Graphical representation of inorganic HTMs vs. PCE in PSCs for the years 2012-2016.[96]

I.6 Challenges of PSCs :

Although the perovskite materials despite having so many advantages these materials too face many challenges. . It depends on numerous factors, both intrinsic, such as perovskite structural and chemical stability and extrinsic, such as moisture ,oxygen, light and heat that limit their life-time to few hundred hours only [97] .The main challenges which are hindering the commercialization of these type of perovskite solar cells listed below:

i) The perovskites employed for manufacturing solar cells are very sensitive to air as air has presence of oxygen and water vapor. The presence of oxygen and water vapor degrade the PV cell as the salt – like crystal structure of perovskite gets dissolved. But this problem has been rectified by researchers as they have addressed that if perovskite films are prepared in an inert atmosphere using boxes filled with Nitrogen or Argon then this problem can be overcome. Further this step is followed by the immediately encapsulating the whole of device in an air tight sealant having the same inert gases . This method of protecting the perovskite from oxidation is not very cost effective when considered for large scale production [98].

ii) The preparation of large continuous films of perovskite in a glove box is also challenging which poses a restriction and limits its production for large scale . But the deposition of the constituent components in a sequential manner can be done to form a thin continuous film for a wider area without degrading the efficiency of the cell [99].

iii) One of the most commonly used material in perovskite based solar cells is lead, which is toxic in nature. Lead can leach out from the panel of solar cell panel into the surroundings into the environment and can cause various ecological and health related challenges. For this very problem an environmentally friendly and benign element like tin has been into the proposition as an alternate source to lead based perovskites [100].

iv) Perovskite based solar cells are reported to possess lower lifetime because of phase transition. Few studies on storage lifetime suggested their operation under sealed conditions at 45°C . Under those conditions the observers observed that the initial PCE was found to be 20 % after 500 h. Much of the work in case of perovskite materials has been done using lead Halides combination. Relatively few work is reported in the field of tin based perovskite films. Owing to the low cost, better stability and also the easy fabrication process of perovskite, the solar cells based on perovskite will be able to contend with the traditional silicon based photo voltaic devices. Also

with their invent solar cell industry has received a new direction to develop highly competent solar cells and panels [101].

v) Severe hysteresis represents another big challenge for perovskites. This is seen in a scan-direction- and scan-speed-dependence to photo J-V characteristics. This behavior makes overestimating the solar-to-electricity efficiency likely. Moreover, the devices with hysteresis also exhibit current degradation when they are operated under the steady-state condition. The hysteresis is likely associated with charge recombination at defective interfaces and grain boundaries[102]. The origins of hysteresis in devices are multifold and are far from well resolved.

Chapter II: Simulation and hole transporting materials

Chapter II: simulation and hole transporting materials

II.1 Introduction:

Computational simulation is a technique of studying and analyzing the behavior of a real device or an imaginary system by mimicking it with a computer application. A simulation is based on a mathematical model that describes the system. Numerical simulation technique of solar cells devices has over the years proven to be a viable tool for studying and understanding the properties of solar cell devices such as the optical, electrical and mechanical properties of complex solar cell devices . In this section, we first described the operation of Solar Cells Capacitance Simulator (SCAPS), which was used to carry out the simulations. Then we presented the mathematical equations which are solved by the software, Operation Theory and Limitations in SCAPS-1D. in the last we talked about Copper based Hole transporting materials for PSCs and there properties.

II.2 Simulation:

Numerical simulation is a crucial and efficient way to investigate the physical mechanism in a solar cell device without actually making the device. It also helps to reduce processing cost and time spent on solar cell device fabrication by providing useful information on how to vary the production parameters to improve the device performance. Many simulations software have been developed and applied in the research of solar cell devices such as AMPS-1D, SCAPS-1D, PC1D, AFORS-HET and so on.

II.3 SCAPS:

SCAPS-1D (Solar Cell Capacitance Simulator) is one-dimensional simulation software developed by the University of Gent, Belgium to simulate the electrical characteristics of different types of solar cells (CZTS, CdTe, CIGS, etc) by solving the basic semiconductor device equations under steady state conditions [103]. In order to simulate a device all the basic input parameters should be well defined so that it behaves as a real counterpart.

The perovskite based solar cells have employed a similar structure with inorganic semiconductor solar cells, such as CIGS. Thus SCAPS can be employed to simulate the perovskite based solar cells [104]. The main features of the latest version of SCAPS, to address the basic parameters, are as follows [103]:

- SCAPS has a very intuitive operation window (Fig. II.1).

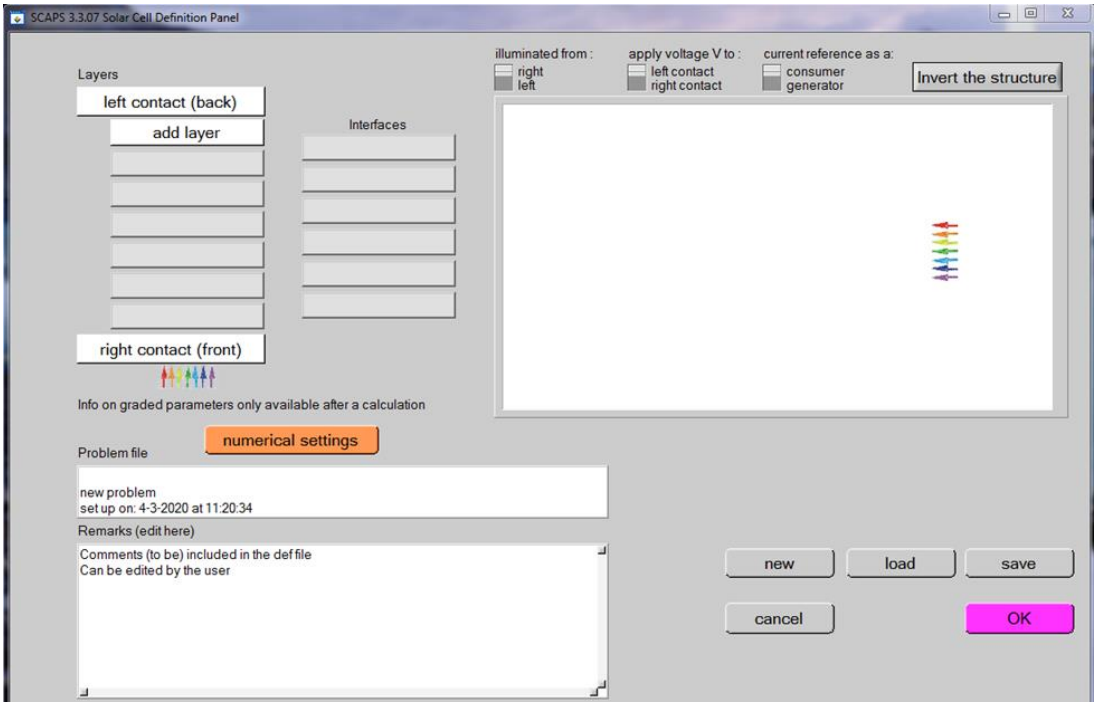

Fig II.1 Layer definition panel in SCAPS-1D.

- Almost all parameters can be graded: band gap (Eg), electron affinity (χ), dielectric constant (ε), valence and conduction band density of states (N_v and N_c), charge carriers mobility (μn and μp), acceptor and donor dopant concentration (N_A, N_D), thermal velocity of charge carriers (Vthn and Vthp), working temperature (T) and absorption constant (α m^{-1}).
- Recombination mechanisms: band-to-band (direct), Auger, SRH-type.
- All traps (defects) Nt can be defined as shown in Figure 2.02. Defect levels: in bulk or at interface; their charge state and recombination is accounted for. Defect levels, charge type: no charge (idealization), monovalent (single donor, acceptor), divalent (double donor, double acceptor, amphoteric), multivalent (user defined), defect levels, energetic

distributions: single level, uniform, Gauss, tail, or combinations are available, defect levels, optical property: direct excitation with light possible (impurity photovoltaic effect, IPV).

- Contacts: work function or flat-band; optical property (reflection of transmission filter) filter.
- Tunneling: intra-band tunneling (within a conduction band or within a valence band); tunneling to and from interface states.
- Generation: either from internal calculation or from user supplied G (x) file
- Illumination: a variety of standard and other spectra included (AM0, AM1.5D, AM1.5G, AM1.5G edition2, monochromatic, white, etc), illumination from either the p-side or the n-side; spectrum cut-off and attenuation.
- Working point for calculations: voltage, frequency, temperature can be chosen by user.
- The program calculates energy bands, concentrations and currents at a given working point, J-V characteristics, C-V, C-f, and QE.
- Batch calculations possible; presentation of results and settings as a function of batch parameters.
- Loading and saving of all settings; startup of SCAPS in a personalized configuration; a script language including a free user function.
- A script language facility to run SCAPS from a "script file"; all internal variables can be accessed and plotted via the script.
- A built-in curve fitting facility.
- A panel for the interpretation of admittance measurements.

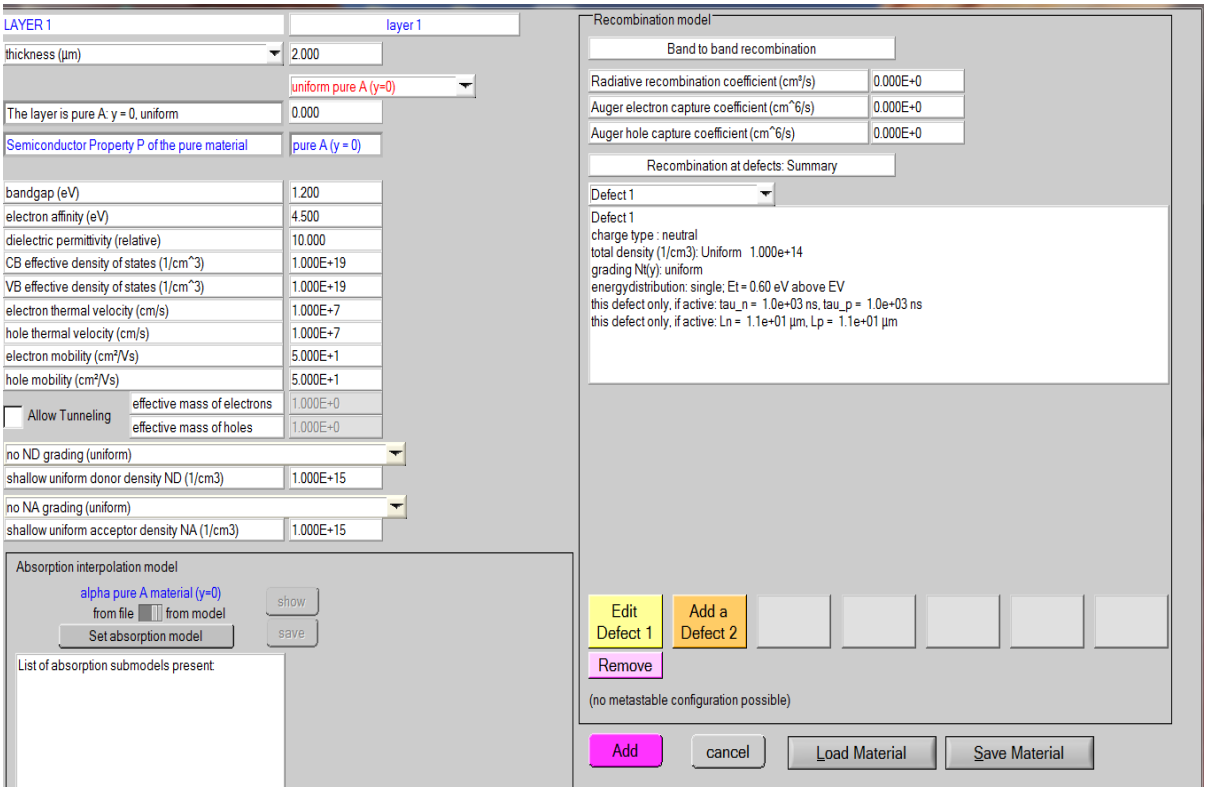

Fig II. 2 Material and defect definition panel in SCAPS-1D.

II.4 Basic Semiconductor Physics in SCAPS-1D:

The simulation is based on the solution of three governing semiconductor equations: Poisson's equation, electron and hole continuity equations. SCAPS numerically solves these three coupled partial differential equations for the electrostatic potentials electron and hole concentration as function of position x.

II.4.1 Basic Equations:

Poisson's equation is used to describe the relationship between potential and space charges, as shown in Eq.2.1

$$\frac{\partial^2}{\partial x^2}\varphi(x) = \frac{q}{\varepsilon}[n(x) - p(x) - N_D^+(x) + N_A^-(x) - p_t(x) + n_t(x)] \qquad (2.1)$$

Where, φ is the potential, q is the elementary charge, ε is the permittivity, n is the density of free electron, p is the density of free hole, N_D^+ is the ionized donor-like doping density, N_A^- is the ionized acceptor-like doping density, p_t is the trapped hole density, n_t is the trapped electron density.

Continuity equations Eq2.2 -2.3 define the transportation of carriers

$$\begin{cases} q\dfrac{\partial n}{\partial t} = \dfrac{\partial J_n}{\partial x} + qG - qR \\ q\dfrac{\partial p}{\partial t} = -\dfrac{\partial J_p}{\partial x} + qG - qR \end{cases} \quad (2.2) \qquad \begin{cases} J_n = qn\mu_n \dfrac{\partial \varphi}{\partial x} + qD_n \dfrac{\partial n}{\partial x} \\ J_p = -qp\mu_p \dfrac{\partial \varphi}{\partial x} + qD_p \dfrac{\partial p}{\partial x} \end{cases} \quad (2.3)$$

Where, G is the optical generation rate, R is the recombination rate, D_n is the electron diffusion coefficient, D_p is the hole diffusion coefficient, μ_n is the electron mobility, and μ_p is the hole mobility.

II.4.2 Concentration of Electrons and Holes:

In thermal equilibrium, the free carrier concentrations are expressed by Eq.2.4-2.5

$$n = N_c \exp\left(\frac{E_f - E_c}{k_B T}\right) \quad (2.4)$$

$$p = N_v \exp\left(\frac{E_v - E_f}{k_B T}\right) \quad (2.5)$$

where, E_f is Fermi level, k_B is Boltzmann constant, T is temperature, E_c and E_v are energy levels under a steady state.

II.4.3 Diffusion Length:

Diffusion length describes the transport ability of carriers in a solar cell device. It depends on diffusion coefficient and carrier lifetime, which is shown in Eq.2.6

$$L = \sqrt{D\tau} \quad (2.6)$$

where, D is the diffusion constant, τ is the carrier lifetime.

II.4.4 Recombination Mechanism:

There are three recombination models used in SCAPS. Band-to-band recombination is a reverse process of photon absorption. The electrons in the conduction band drop back down to the empty valence band and recombine with holes. The band-to-band recombination rate can be expressed as:

$$R = \gamma(np - n_i^2) \qquad (2.7)$$

The Shockley-Read-Hall (SRH) recombination is also called trap-assisted recombination. It occurs due to the defects or impurities in the materials. The SRH recombination rate can be given by:

$$R = \frac{np - n_i^2}{\tau_p(n - n_0) + \tau_n(p + p_0)} \qquad (2.8)$$

Auger recombination is a process when a pair of electron and hole recombination occurs during the transition from high energy level to low energy level, with the resulting energy being given to the third carrier. It can be described by:

$$R = \left(c_n^A + c_p^A\right)(np - n_i^2) \qquad (2.9)$$

where, R is recombination rate, γ is recombination coefficient, τ_n and are τ_p lifetimes for electron and hole, n_0 and p_0 are equilibrium electron concentration and equilibrium hole concentration, c_n^A and c_p^A are constants, which can be set in SCAPS.

II.4.5 Work Function:

Work function is the minimum energy required to move an electron from a solid to vacuum.

The value of work function is used to describe the strength of binding energy of an electron in materials. In SCAPS, work function can be set by the user, or it can be calculated by using the model in SCAPS, as shown in Eq.2.10-2.12

n-type contact:

$$\phi_m = \chi + k_B T ln\left(\frac{N_c}{N_D - N_A}\right) \qquad (2.10)$$

p-type contact:

$$\phi_m = \chi + E_{gap} - k_B T ln\left(\frac{N_C}{N_A - N_D}\right) \quad (2.11)$$

intrinsic contact:

$$\phi_m = \chi + k_B T ln\left(\frac{N_c}{n_i}\right) \qquad (2.12)$$

where, ϕy is work function, χ is electron affinity, Nc is effective density of state for conduction band, NA and ND are acceptor and donor dopant densities. Ni is intrinsic carriers' densities.

II.4.6 Absorption Coefficient:

The absorption coefficient can be defined as the extent to which a material absorbs energy. It is determined by the nature of material. In SCAPS, the absorption coefficient is given by Eq.2.13

$$\alpha(\lambda) = \left(A + \frac{B}{h\nu}\right)\sqrt{h\nu - E_{gap}} \qquad (2.13)$$

where, A and B are the absorption constants, h is Planck's constant, v is light speed.

II.4.7 Operation Theory:

The main theory of SCAPS-1D is to solve Poisson's equation and continuity equations. Fig.2.3 shows the working strategy of SCAPS-1D. Each calculation begins from the start point, and uses the initial assumption, which is expressed by using quasi-Fermi levels, to obtain the equilibrium situation. In this situation, no illumination and voltage are applied. When the working point is set in a dark condition, the equilibrium condition is applied to calculate the solution.

When it is set under a light condition, the short circuit situation will be calculated, and this new value will be used as the initial value of the next step[103].

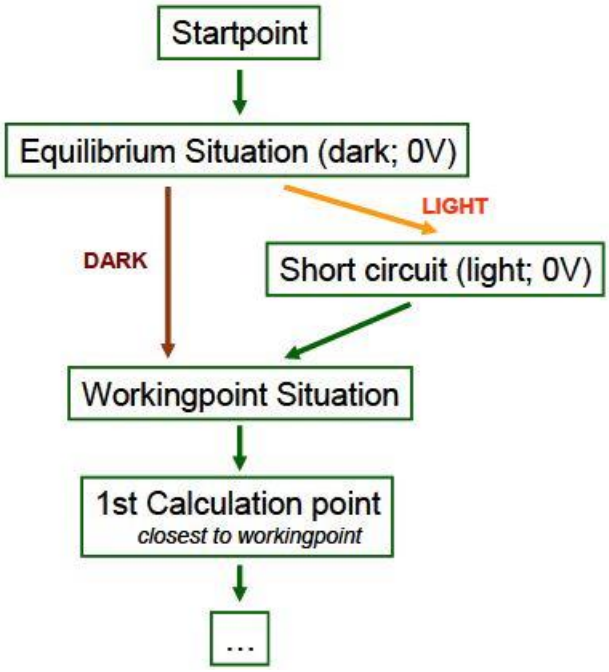

Fig II.03 Working Strategy of SCAPS-1D[103].

The convergence of the Gummel type iteration scheme with Newton-Raphson algorithm is used in SCAPS for numerical calculations. After a calculation point is set, SCAPS will follow Newton-Raphson algorithm to undertake iteration calculation until obtaining the optimization value.

II.4.8 Limitations in SCAPS-1D:

There are three limitations in the SCAPS-1D. Firstly, the device model can only add seven semiconductor layers. Due to this reason, SCAPS-1D is not suitable for a device with graded junctions. Another limitation is that SCAPS-1D is developed for thin film solar cells, so it cannot be applied for other device structures, such as a perovskite solar cell with mesoporous structure. The last limitation is about the accuracy of calculation. Although the resolution is already a small number ($<10^{-15}$), it is usually insufficient for the simulation of semiconductors[105].

II.5 Copper based Hole transporting materials for PSCs:

Copper based inorganic p-type semiconductors, such as copper iodide (CuI), copper thiocyanate (CuSCN), copper oxide (CuO) and cuprous oxide (Cu_2O), have several unique properties, including ease of fabrication correlated with low production cost, suitable band alignment with perovskite active layer, high hole mobility/conductivity, solution processability and high chemical stability. These merits make the Cu based p-type semiconductors promising HTM candidate materials that can be explored in PSCs.

II.5.1 Copper iodide (CuI) :

The CuI was selected because of its inexpensive cost, stability, higher p-type conductivity, and suitable level valence band. Moreover, the inorganic CuI has great compatibility with perovskite, thereby resulting in the fast hole transfer from the perovskite to the CuI layer. Impedance spectra indicated that the electrical conductivity of the CuI is one hundred times higher than that of the spiro-OMeTAD. CuI was found to suffer from the low V_{oc} of less than 0.6 V which was related to a recombination issue due to free iodine in the CuI layer inducing valence band trap states. High hole mobility of CuI which is five orders of magnitude greater than that of spiro-OMeTAD still encourages its use in PSCs [106].

II.5.2 Copper thiocyanate (CuSCN):

The Key to success is the incorporation of the wide bandgap p-type semiconductor copper thiocyanate (CuSCN), as the hole-transporting, electron blocking material. In addition to its excellent and strictly unipolar transport properties, CuSCN is a superb hole-transport layer (HTL) choice due to its low cost, nontoxicity, and annealing temperature, its chemical stability and its compatibility with a range of solution-processing methods. The role of CuSCN is to selectively transport holes to the anode while blocking electrons and hence minimizing recombination losses at the semiconductor/anode interface [107].

II.5.3 Copper oxide (CuO):

the copper oxide as the hole transport material is proposed in the structure of the PSCs. CuO has a higher conductivity, and hence higher current density, than the other HTMs such as spiro-OMeTAD that having smaller molecular size, which allows a higher fill factor (FF). Cupric oxide has a band gap of 1.21–2.1 eV and a monoclinic crystal structure. In addition, CuO exhibits excellent durability as a result of their environment-friendly nature. The chemical stability tests showed that the CuO does not allow water to spread in the material as spiro-OMeTAD. Moreover, the light absorption of CuO in the entire visible spectrum is more than in the narrow-bandgap spiro-OMeTAD. Moreover, CuO is mechanically stronger and is more resistant to serration and scratching [108].

II.5.4 Cuprous oxide (Cu_2O):

Cuprous oxide (Cu_2O), a direct-gap semiconductor with band-gap energy of 2.2–2.9 eV and a cubic crystal structure, has been regarded as one of the most promising materials for application to photovoltaic cells. The attractiveness of Cu_2O as a photovoltaic material lies in the fact that the constituent materials are nontoxic and abundantly available on the earth, and that the Cu_2O has a high absorption coefficient in visible regions and low-cost producibility[109].

Chapter III: Results and discussion

Chapter III: Results and discussion

III.1 Introduction:

The organic-metal halide perovskite is emerging technology in photovoltaic solar cells. For any solar cell to get the significant efficiency depends on various design parameters such as material thickness, device architecture, doping concentration etc. Some reports showed that the HTM layer affects the device performance and the degradation of device performance was observed by using organic material as HTM. Therefore, in order to commercialize the perovskite solar cells and dominate the photovoltaic industry, it is necessary to find an alternative HTM layer for PSCs. Inorganic materials especially Cu-based materials are considered as promising materials for the HTM layer because of their favorable characteristics, such as high mobility of hole, low cost of fabrication, better chemical stability, and appropriate valance band position. In this chapter we studied the influence of HTM layer and other characteristics on perovskite solar cell to get optimum design and high-performance perovskite solar cell. Here for this research, we used SCAPS-1D because it is freely available, simple, efficient and quite popular in solar cell research society.

III.2 Device structure:

In this work, numerical modeling of the Perovskite solar cell (PSC) and calculation of its parameters were performed using 1D-Solar Cell Capacitance Simulator (SCAPS-1D). These calculations are performed on the basis of three basic equations that are: (i) hole continuity equation (ii) electron continuity equation and (iii) Poisson equation. The structure of the solar cell consists of Glass FTO/TiO_2/$CH_3NH_3PbI_3$/Cu-based HTL/Au, as illustrated in Fig III.1. Here HTL refers to a hole transporting layer. The multilayer PSC architecture is a planar n-i-p structure where the intrinsic $CH_3NH_3PbI_3$ layer is inserted between the p-type HTL and the n-type TiO_2. The back contact is gold (Au), and the front contact is fluorine doped tin oxide (FTO) which is a transparent conducting oxide. A schematic view of the simulated PSC in this work is shown in Figure III.1.

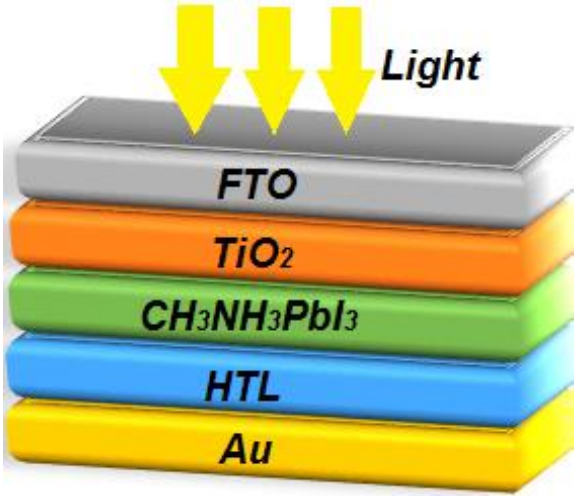

Fig III.1 Schematic view of the perovskite solar cell structure simulated in this work.

III.3 Simulation parameters:

The parameters and characteristics of the different materials used in SCAPS-1D for simulation are adopted from literature [110–115] and are summarized in Tables III.1, III.2, III.3 and 3.4. In the device simulation, HTM / $CH_3NH_3PbI_3$ and CH_3NHPbI_3 / ETM interface defect layer are also considered to take into account the interface recombination due to interface defect density. All the simulations are carried out at a temperature of 25 °C and an air mass of AM1.5 G (illumination of 1000 W/m^2).

Parameter	Symbol	ETM (TiO_2)	Perovskite($CH_3NH_3PbI_3$)
Thickness	d (μm)	0.05	0.40
Band gap	Eg (eV)	3.20	1.55
Affinity	χ (eV)	3.90	3.90
Relative dielectric permittivity	ε_r	9.00	6.50
Effective density of states at CB	N_c (cm^{-3})	$1\times10^{+21}$	2.2×10^{18}

Effective density of states at VB	N_v (cm^{-3})	2×10^{20}	1.8×10^{19}
Mobility of electrons	μ_n (cm^2 /V.s)	20	2
Mobility of holes	μ_p (cm^2 /V.s)	10	2
Density of n-type doping	N_d (cm^{-3})	1×10^{19}	5.21×10^{9}
Density of p-type doping	N_a (cm^{-3})	0	5.21×10^{9}
Density of defects	N_t (cm^{-3})	1×10^{15}	2.5×10^{13}

Table III.1 Parameters used for simulation of perovskite solar cell structures using SCAPS-1D.

Parameter	CuSCN	CuI	CuO	Cu_2O
d (μm)	0.05	0.05	0.05	0.05
Eg (eV)	3.40	2.93	1.51	2.17
χ (eV)	1.90	2.10	4.07	3.20
ε_r	10.00	6.50	18.10	7.11
N_c (cm^{-3})	1.7×10^{19}	2.8×10^{19}	2.2×10^{19}	2.02×10^{17}
N_v (cm^{-3})	2.5×10^{21}	1×10^{19}	5.5×10^{20}	1.1×10^{19}
μ_n (cm^2 /V.s)	1×10^{-4}	1.69×10^{-4}	1×10^{2}	2×10^{2}
μ_p (cm^2 /V.s)	1×10^{-1}	1.69×10^{-4}	1×10^{-1}	8×10^{1}
N_d (cm^{-3})	0	0	0	0
N_a (cm^{-3})	1×10^{18}	1×10^{18}	1×10^{18}	1×10^{16}
N_t (cm^{-3})	1×10^{14}	1×10^{15}	1×10^{14}	1×10^{14}

Table III.2 Parameters used for simulation of the HTL materials used.

Interface layer	HTM/perovskite layer	Perovskite layer/ETM
Defect type	Neutral	Neutral
Capture cross section electrons (cm^2)	1×10^{-18}	1×10^{-15}
Capture cross section holes (cm^2)	1×10^{-16}	1×10^{-15}
Energetic distribution	Single	Single
Reference for defect energy level Et	Above the highest Ev	Above the highest Ev
Energy with respect to reference (eV)	0.05	0.60
Total density ($1/cm^2$)	1×10^{12}	1×10^{11}

Table III.3 Parameters of interface layers.

Parameters	Back contact	Front contact
Surface recombination velocity of electrons(cm/s)	1×10^{5}	1×10^{5}
Surface recombination velocity of holes (cm/s)	1×10^{7}	1×10^{7}
Metal work function (eV)	5.1	4.3

Table III.4 Parameters of contacts.

III.4 Results and discussion:

III.4.1 Effect of different Cu-based HTLs:

Organic HTMs guaranteeing high PCE of PSCs, but the necessity of external doping make them more prone to degradation over time under humidity. Furthermore, manufacturing cost plays an important role in commercializing PSC, while most of organic HTMs are too expensive. Therefore, it is dire need to replace costly and unstable HTMs with a cost effective and stable HTM having

high hole mobility with ease of synthesis. Inorganic p-type semi-conductors such as copper (Cu) based materials are considered to be an alternative of organic HTMs.

Fig III.2 (a) illustrates the performance of the solar cell for different HTLs, the current density–voltage (J-V) characteristics. The quantum efficiency (QE) curves of the proposed PSCs are illustrated in Fig III.2 (b) depicting that the various studied PSCs show the same QE curve with slight differences. The QE curve is covered over almost the entire visible range of the solar spectrum. The QE is nearly constant from 350 nm to 550 nm and then it decreases till 800 nm.

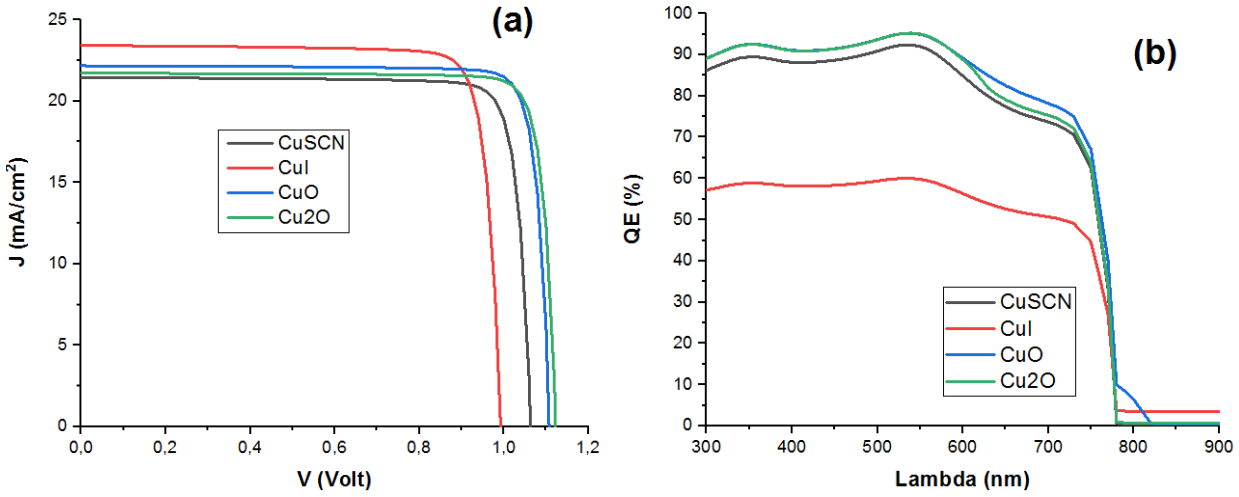

Fig III.2 (a) Effect of different HTLs on IV measurements, **(b)** Effect of different HTLs on QE.

We extracted the device performance parameters such as short-circuit current density Jsc, open-circuit voltage Voc, fill factor FF, and power conversion efficiency PCE of the proposed PSC with copper (Cu) based HTLs from the J-V characteristics and the results are shown in Table III.5.

HTL	Voc (V)	Isc (mA/cm^2)	FF (%)	eta (%)
CuSCN	1.06	21.44	86.65	19.78
CuI	0.99	23.42	85.31	19.86
CuO	1.08	21.40	86.91	20.05

Cu_2O	1.12	21.56	87.71	21.24

Table III.5 Effect of different HTLs on solar cell parameters.

The PSC with Cu_2O as HTL shows the highest PCE of 21.24% with the highest Voc and FF. We know that in order to reduce energy loss and obtain high device performance, it is expected to have a small valance band offset (-0.2 eV to 0.2 eV) between the HTM layer and the perovskite layer. Thus, Cu_2O have an appropriate valance band position, and the value of valance band offset of Cu_2O is less than 0.1 eV. In addition, Cu_2O exhibits a high hole mobility up to 80 $cm^2.V.s^{-1}$ compared with organic materials (Spiro-OMeTAD 0.0001 $cm^2.V.s^{-1}$). Therefore, for all these reasons that have been mentioned, it is believed that Cu_2O is the probable alternative material that can be utilized in HTM layers.

In our simulation model it is clear therefore that Cu_2O as the best HTM among the HTL material proposed.

III.4.2 Effect of different back contacts:

The main obstacle that is hindering PSC to commercialize is high cost and low thermal stability of back contact. It is required to have a suitable work function material as back contact so that it may yield reasonable built in voltage.

To get a suitable back contact for our device simulations, have been carried out using different materials: silver (Ag), iron (Fe), copper (Cu) graphite alloy, nickel (Ni), and platinum (Pt) as prospective back contact for perovskite solar cell and compared to the initial back contact (gold (Au)). Values of different back Metal work function (Φm) are summarized in Table III.6.

Back contact Material	Au	Ag	Fe	Cu-graphite alloy	Ni	Pt
Metal work function,Φm(eV)	5.10	4.74	4.81	5.00	5.50	5.70

Table III.6 Metal work function of different back contacts.

From the simulation it was observed that the metal work function has influence on JV curve (as shown in figure III.3(a)). The S-shaped curve for lower work function materials is due to the large barrier at Cu_2O/back contact interface which hinders the injection of hole to the back contact. The quantum efficiency (QE) curves of the proposed PSC with different back contacts are illustrated in Figure III.3(b) depicting that the various studied PSCs show that QE increase with the increase of Φm and it became the same when Φm ≥ 5 eV .

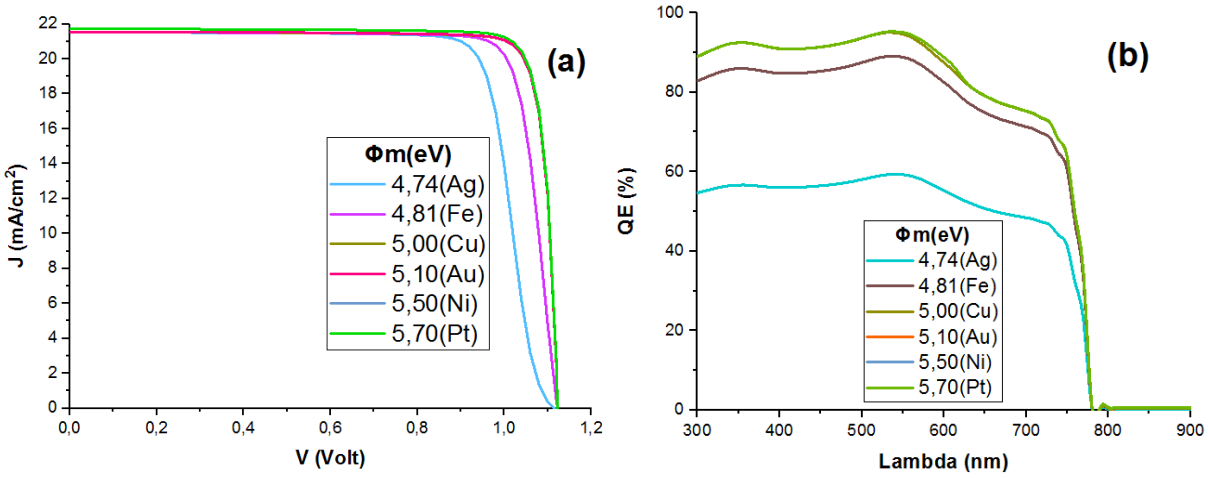

Fig III.3 (a) effect of different back contacts on IV measurement, **(b)** effect of different back contacts on QE.

Increasing the back contact Schottky barrier (formed at Cu_2O/back contact interface) (Φm) from 4.74 eV to 5.7 eV, V_{oc} increased from 1.11 V to 1.12 V and after 5.0 eV it is saturated as shown in Fig III.4. J_{sc} was increased from 21.51 mA/cm^2 to 21.72 mA/cm^2.

It is also clear that PCE and FF of the PSC depends significantly on the back contact work function, because with the increase in Φm which results in easy hole transport from Cu_2O to back contact

and therefore FF and PCE increases. Thus, back contact work function greater or equal to 5 eV is necessary to get high solar cell performance.

Here, therefore, it is opted Cu-graphite alloy with work function 5 eV as a back contact in our simulation model because of its low cost and favorable work function.

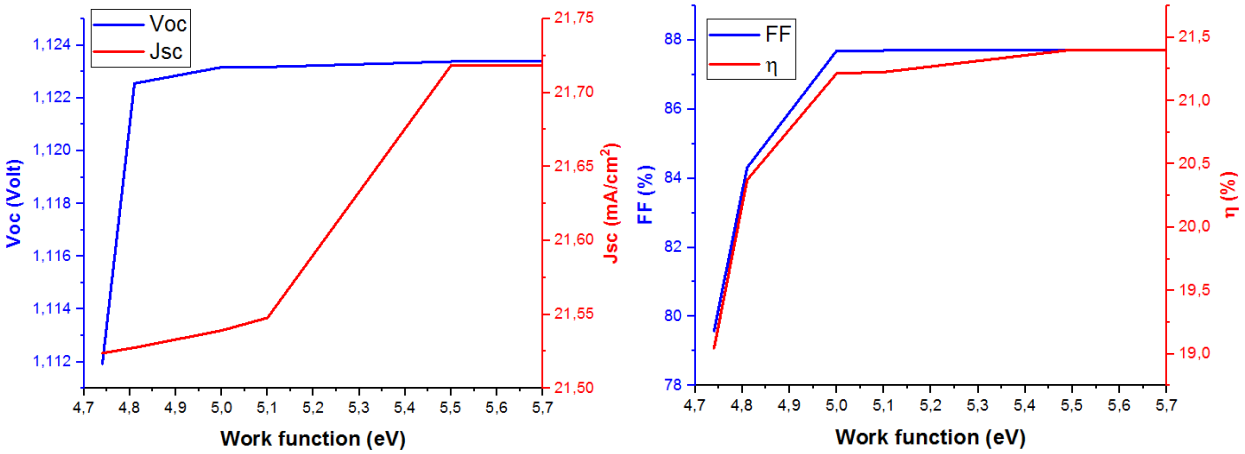

Fig III.4 Effect of different back contacts on solar cell parameters.

III.4.3 Effect of $CH_3NH_3PbI_3$ layer:

III.4.3.1 Effect of thickness of $CH_3NH_3PbI_3$ layer :

To examine the influence of thickness of $CH_3NH_3PbI_3$ absorber layer, simulation was carried out at different thickness varying from 100 nm to 1000 nm by keeping all other parameters the same as in Table III.1.

As shown in Fig.3.5(a), the JV-curve obtained after simulation states that on increasing the thickness of absorber, increases with increasing thickness.

The external quantum efficiency of the device first increases rapidly up to 600 nm and after it gets increased slowly as shown in Fig III.5(b). To absorb the maximum number of photons and to generate electron-hole pair, absorber layer should be set to an optimum thickness, keeping in mind the short diffusion length and higher defect density in thicker perovskite.

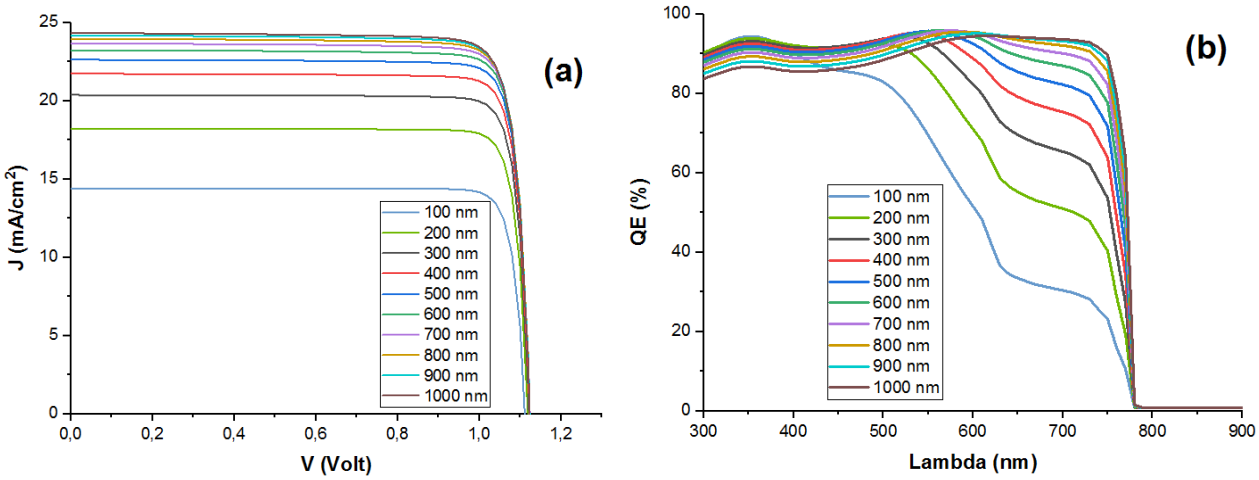

Fig III.5 Effect of the perovskite thickness of on IV characteristics **(a)** and QE **(b)**.

Figure III.6 (a) demonstrates that J_{sc} increased significantly from 14.42 mA/cm^2 to 23.24 mA/cm^2 as the thickness was increased from 100 nm to 600 nm and after that it increased slowly (from 23.24 mA/cm^2 to 24.62 mA/cm^2). As the thickness of absorber was increased, J_{sc} kept on increasing because of absorption of more photons with longer wavelength in thicker perovskite. V_{oc} was increased by very small amount (0.02 eV) with the increase in thickness, and then it became constant after the thickness rich 300 nm.

The FF decrease monotonically (from 88.67 % to 84.04 %) with the increase in the absorber layer thickness. This happened because the forward bias voltage reduces the electric field leading to an increase in recombination of current in absorber. The PCE of the device increased rapidly (from 14.22 % to 22.24 %) with increasing thickness up to perovskite thickness of 500 nm and after 500 nm it increased slightly.

600 nm thickness of absorber is suitable to get optimum values of solar cell parameters at which FF and PCE were 87.16 % and 22.78 % respectively.

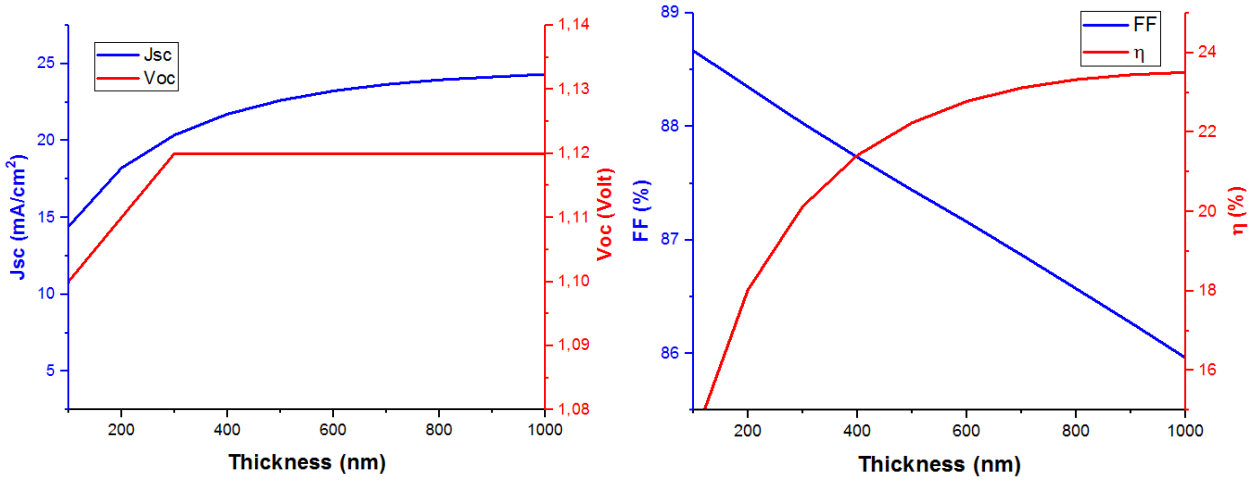

Fig III.6 Effect of thickness of perovskite on solar cell parameters.

III.4.3.2 Effect of defect density in perovskite layer:

When sunlight is incident on PSCs, photo-generated carriers (electron and holes) are generated on the absorber layer. These photogenerated carriers are subsequently collected by the electrode and transfer towards the external current. During the collection of photo-generated charge carriers, a large number of carriers is lost due to the poor quality of perovskite layer. Higher defect density causes higher recombination rate in the low-quality perovskite films that leads to reduce the diffusion length of charge carriers as well as the life time of carriers It also leads to higher rate of degradation of film and it also reduces stability and overall performance of the device.

To estimate the optimum defect concentration in the absorber for optimum parameters, simulation was carried out by varying the defect density from $1x10^{12}$ cm^{-3} to $1x10^{16}$ cm^{-3}.

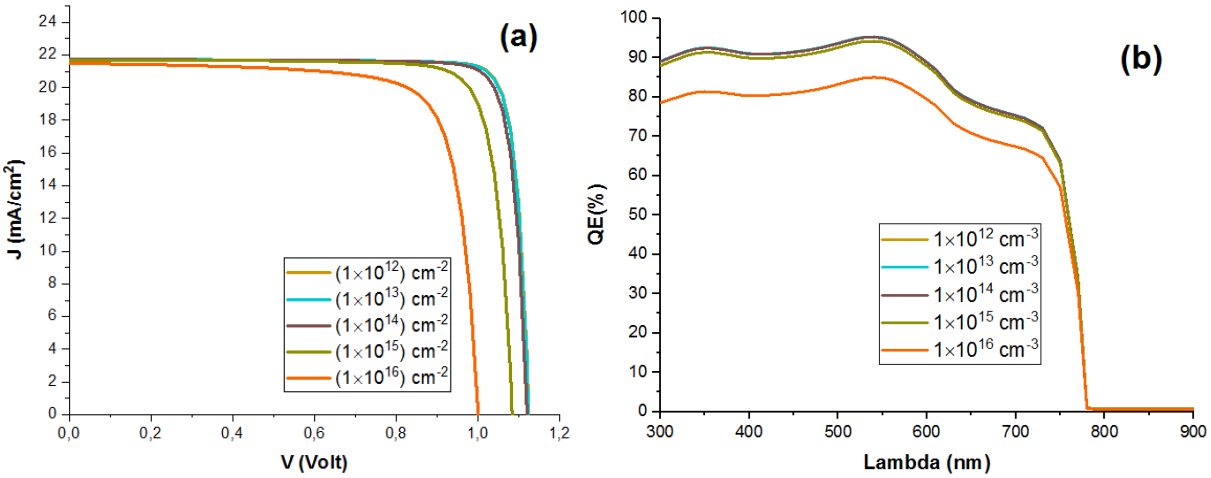

Fig III.7 Effect of defect density in perovskite layer on IV characteristics **(a)** and QE **(b)**on.

All the parameters, as shown in Fig III.8 of the device, are reduced significantly as the defect concentration in the absorber layer was raised above $1x10^{13}$ cm^{-3}. A large number of defect density leads to an increased rate of recombination which leads to the reduction in the diffusion length of charge carriers ultimately and life-time of carriers will be decreased. Thus, to obtain higher efficiency the defects in perovskite should be reduced to 1.10^{13} cm^{-3} or less by improving the crystal structure and processing method but to obtain this in practical at 600 nm perovskite thickness is impractical so the optimized defect density at optimum thickness is considered to be of the order of $1x10^{14}$ cm^{-3}. A promising PCE and FF of 21.13% and 86.91% were obtained at defect density $1x10^{14}$ cm^{-3} respectively.

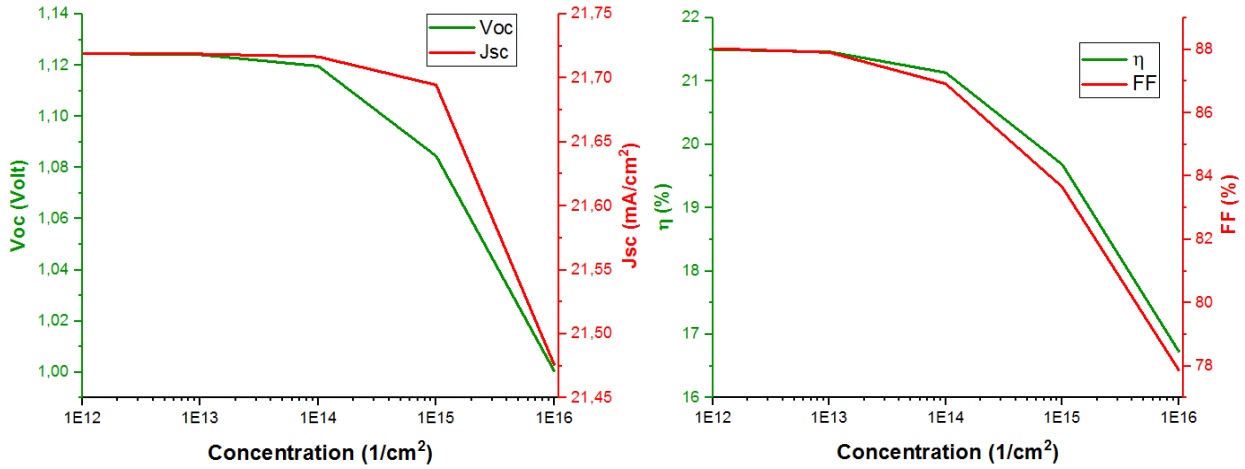

Fig III.8 effect of defect density in perovskite layer on solar cell parameters.

III.4.4 Effect of HTL layer (Cu_2O):

III.4.4.1 Effect of thickness of HTL layer (Cu_2O):

A key function of the HTL is to transport the photogenerated holes to the counter electrode. If the thickness of the HTL is small, the distance traveled by the holes to reach the electrode will be minimized leading to reduce the recombination probability. However, thinner HTL should be avoided because it could reduce the uniformity of coverage on the perovskite surface. On the other hand, thicker HTL causes higher series resistance. So, there is an optimum choice for the thickness to give the best performance.

Simulation was done at different thicknesses varying from 00 nm to 800 nm. Fig III.9 shows the effect of thickness of Cu_2O layer on (a) J-V and (b) QE curves.

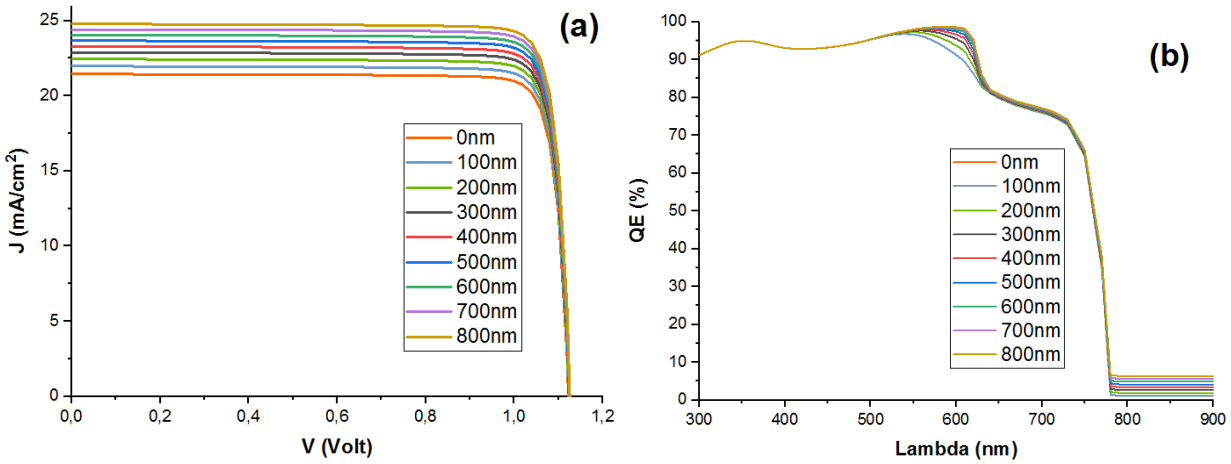

Fig III.9 Effect of thickness of HTL layer (Cu_2O) on J-V characteristics **(a)** and QE **(b)**.

According to Fig III.10, it is observed that V_{oc} increases as the thickness of the hole transport layer is increased but the increment is very small. The same behavior is noticed for the fill factor but in a less manner with the thickness increment. J_{sc} and PCE increase from 21.45 mA/cm^2 to 22.88 mA/cm^2 and from 21.16 % to 22.6 % respectively as the thickness increases from 0 nm to 300 nm, after that the increase rate is reduced slightly. The results show that no HTL or a very thin is not suitable for high efficiency. If the thickness is less than the ideal thickness, HTL may not cover the perovskite crystals completely. A thin HTL does not cover perovskite layer completely and chances of recombination are high because path length for charge carriers is increased to reach the back

electrode thereby increasing series resistance. So, the best performance is selected when the thickness of HTM is 300 nm with a PCE of 22.6 %, FF of 87.79 %, Voc 1.123 V, and Jsc of 22.88 mA/cm^2 compared to the initial design.

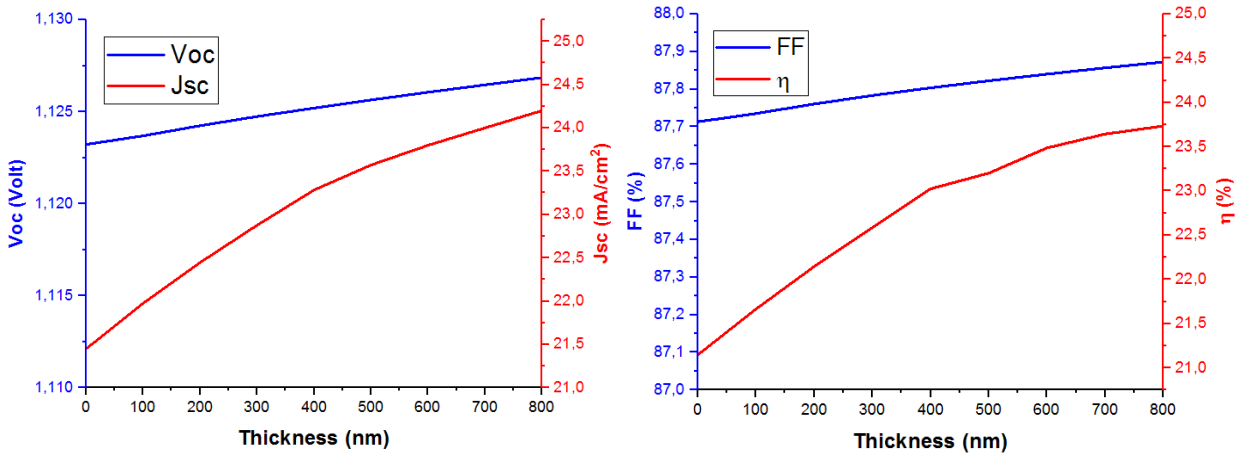

Fig III.10 Effect of thickness of HTL layer (Cu_2O) on solar cell output parameters.

III.4.4.2 Effect of doping concentration of HTL layer (Cu_2O):

To investigate the influence of doping concentration of Cu_2O on the device performance, the acceptor doping concentration was varied from 1x10^{14} cm^{-3} to 1x10^{21} cm^{-3}. As shown in Fig.3.9, doping concentration has no influence on neither JV nor QE curves (as shown in Fig III.11).

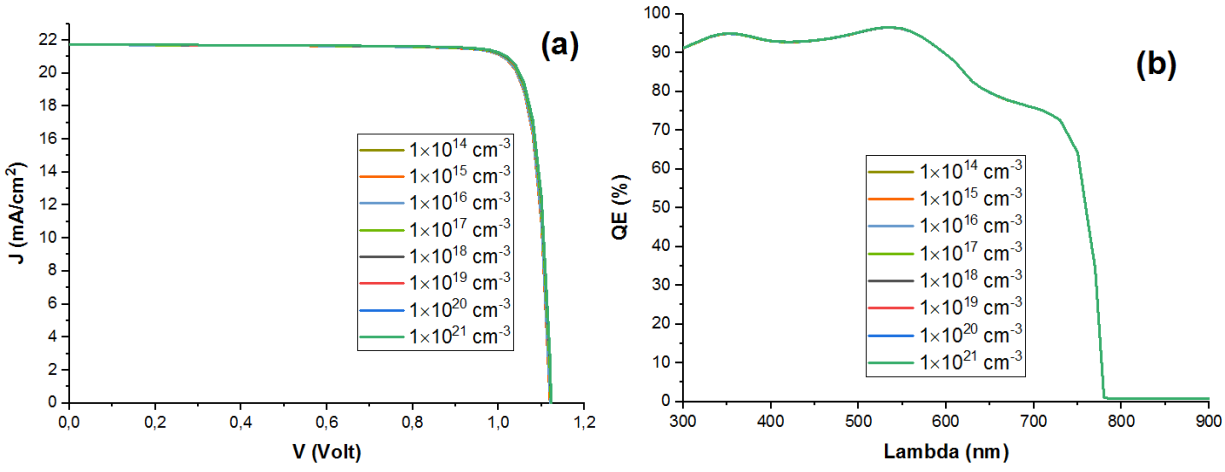

Fig III.11 Effect of doping concentration of HTL layer (Cu_2O) on J-V characteristics **(a)** and quantum efficiency QE **(b)**.

In Fig III.12, V_{oc} and J_{sc} remained nearly unchanged under any variation in doping concentration. It is clear that PCE increases (from 21.21 % to 21.42 %) up to doping concentration of $1x10^{19}$ cm^{-3} and then it saturates. FF also changed in a similar fashion to PCE (from 87.28 % to 87.78 %). As the doping concentration is increased, resistivity decreased which caused increment in FF and the overall device performance. The difference between the energy bands of the Cu_2O and the absorber layer increases with the increase of doping concentration; so, the electric potential is enhanced meaning that the electric field can speed the separation of the photon-generated carriers which, in turn, reduces the recombination rate and improves the cell performance. In addition, high acceptor density can generate deep Coulomb traps and, in turn, deteriorate hole mobility. $1x10^{19}$ cm^{-3} acceptor concentration of Cu_2O layer is enough to get desirable device performance.

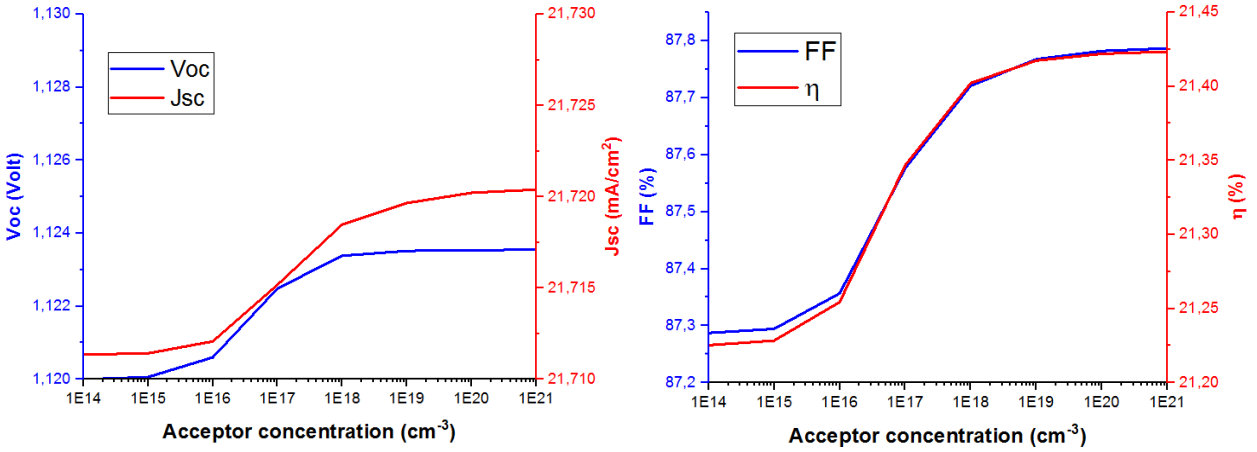

Fig III.12 Effect of doping concentration of HTL layer (Cu_2O) on solar cell output parameters.

III.4.5 Effect of (TiO_2 / $CH_3NH_3PbI_3$) and (Cu_2O / $CH_3NH_3PbI_3$) interface layers:

The interface has a great importance for a photovoltaic device since it usually is full of defects due to the material discontinuity. The performance of perovskite solar cells can be altered (in most cases negatively) by defect states. The perovskite deposition process may induce defects at interfaces and grain boundaries. The formation of these defects can also be due to the interaction of precursor solvents with HTL and ETL.

III.4.5.1 Effect of (Cu_2O / $CH_3NH_3PbI_3$) defect interface:

To investigate the influence of defect on solar cell performance at this interface, the neutral defect density to this interface was varied from $1x10^8$ cm^{-2} to $1x10^{13}$ cm^{-2}. The JV curve obtained is shown in Fig III.13(a). The curve decreases from the voltage side as the defect density increases. The quantum efficiency (QE) curves are illustrated in Fig III.13(b). It is observed that the increase of (Cu2O / CH3NH3PbI3) defect interface has a small effect on the QE curve.

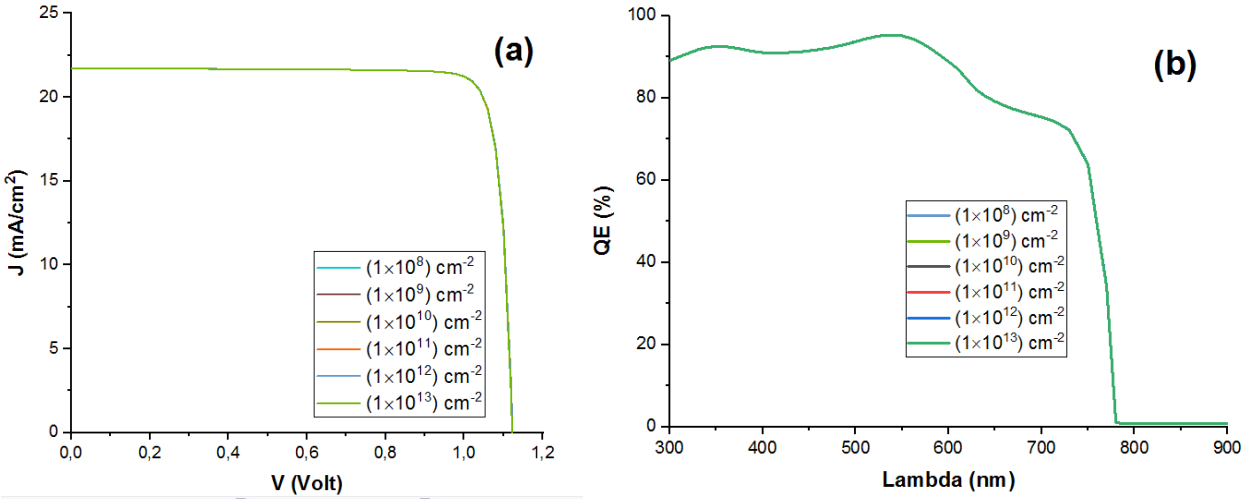

Fig III.13 Effect of (CuSCN / $CH_3NH_3PbI_3$) defect interface on J-V characteristics **(a)** and QE **(b)**.

By observing Fig III.14, it is noticed a slight decrease in Voc (0.001 V) with increase in defect density up to $1x10^{12}$ cm^{-2} while Jsc remains unchanged. PCE and FF are reduced from 21.40 % to 21.38 % and from 87.72 % to 87.71 % respectively on increasing defect at this interface. Thus, it is observed that defects at $CH_3NH_3PbI_3/Cu_2O$ interface don't have much effect on the device performance.

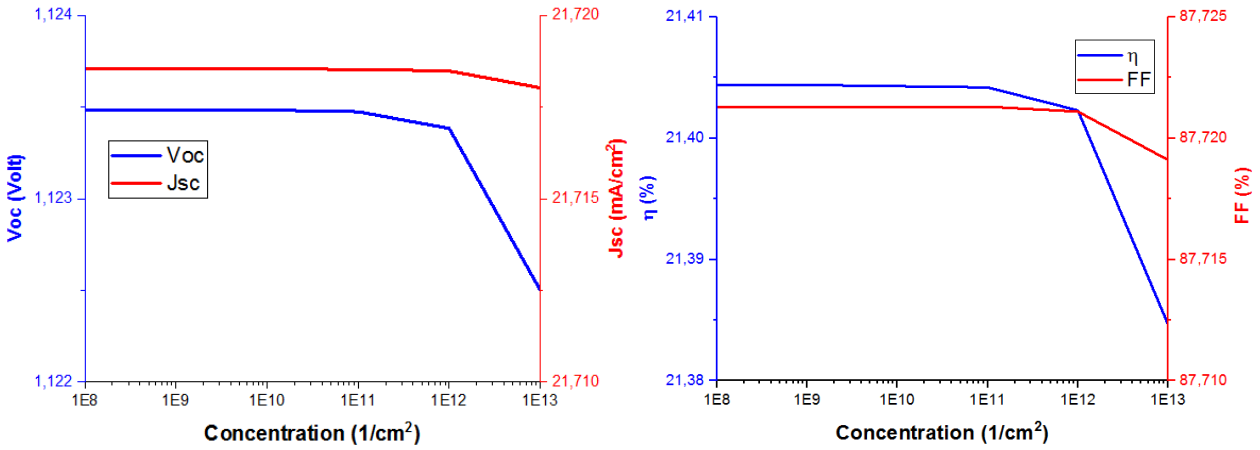

Fig III.14 effect of (CuSCN / $CH_3NH_3PbI_3$) defect interface on solar cell parameters.

III.4.5.2 Effect of (TiO_2 / $CH_3NH_3PbI_3$) defect interface:

To monitor how the interface states have impact on perovskite solar cell efficiency the ETM-Perovskite interface defect levels are varied from $1x10^{10}$ cm^{-2} to $1x10^{15}$ cm^{-2} along with the perovskite layer bulk defects variation to observe the cumulative effect on cell PCE.

J-V characteristics and QE curves of the perovskite solar cells with varied defect densities are depicted in Figure III.15 (a) and (b) respectively.

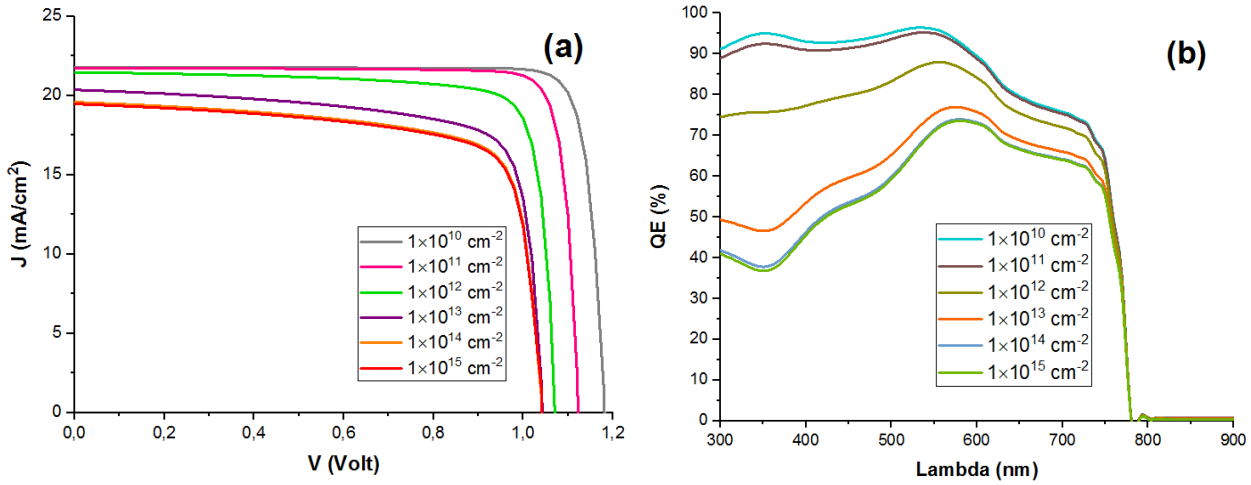

Fig III.15 Effect of (TiO_2 / $CH_3NH_3PbI_3$) defect interface on J-V characteristics **(a)** and QE **(b)**.

By observing fig III.16, it is clear that the PSC fill factor is highly affected by the increment of defect state in (TiO_2 / $CH_3NH_3PbI_3$). The cell efficiency goes significantly downward from 22.59 % to 16.16 %, when defect density is increased from $1x10^{10}$ cm^{-3} to $1x10^{13}$ cm^{-3}. In the range of defect state density $1x10^{13}$ ~ $1x10^{15}$ cm^{-3}, device efficiency changes a little (16.16 % to 15.18 %). FF decreases from 88.18 % to around 75.23 % and then it became nearly unchanged when the density of the defect interface achieves the value $1x10^{13}$ cm^{-3} or more.

In the case of V_{oc}, it has been observed that it drops from 1.17 V to 1.0 V when defect density is increased from $1x10^{10}$ cm^{-3} to $1x10^{13}$ cm^{-3}. The simulation shows that density of defect has impact on J_{sc}. It decreased from 21.71 mA/cm^2 to 19.46 mA/cm^2 when the concentration of defects is up to $1x10^{11}$ cm^{-3}.

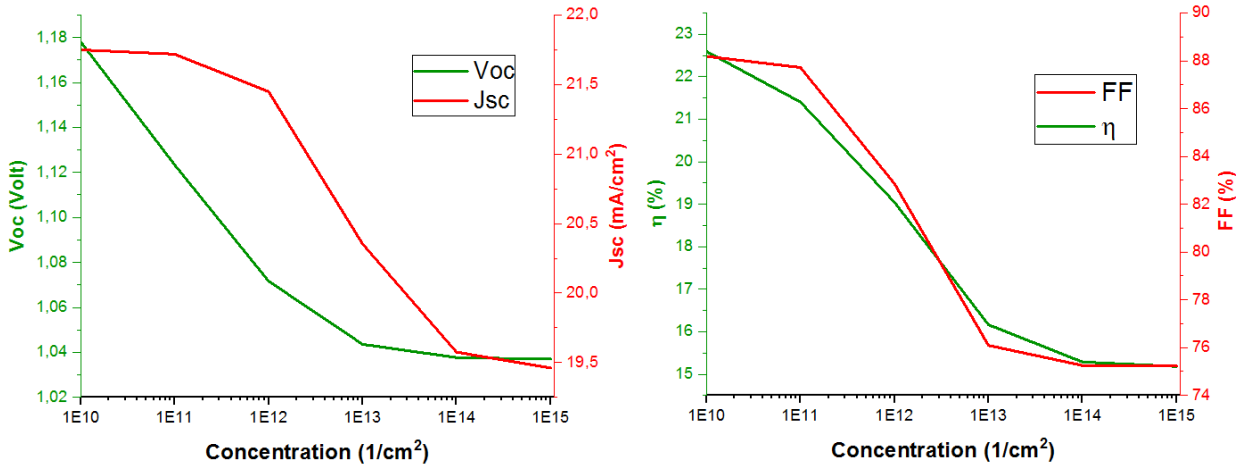

Fig III.16 Effect of (TiO_2 / $CH_3NH_3PbI_3$) defect interface on solar cell parameters.

III.4.6 Simulated device with optimized parameters:

The effect of all the simulated parameters has been calculated by keeping others constant. In this section the overall device performance parameters are simulated by considering all the parameters interconnected together. Figure III.17 shows the final device structure obtained using the optimum values of different electrical parameters found through our simulation.

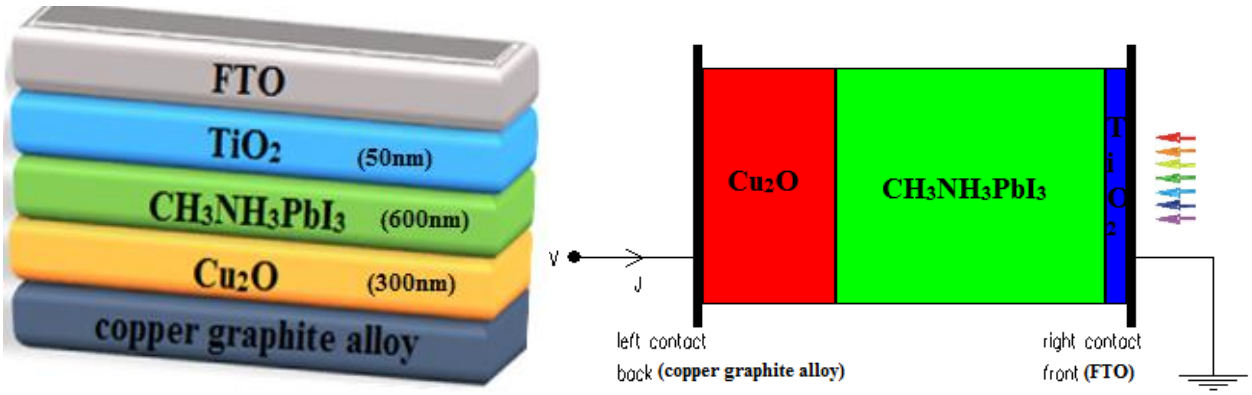

-(a)- **-(b)-**

Fig III.17 Architecture of simulated model **(a)** and Device structure depicted by SCAPS3.3.07 **(b)**.

Table III.7 summarizes the optimum parameters for the simulated solar cell and the other parameters stay the same as .

	Thickness	Doping concentration	Defect density
Cu_2O	300nm	1.10^{19}	1.10^{14}
$CH_3NH_3PbI_3$	600nm	/	1.10^{14}
(Cu_2O /$CH_3NH_3PbI_3$)	/	/	1.10^{12}
(TiO_2 /$CH_3NH_3PbI_3$)	/	/	1.10^{10}

Table III.7 Optimized parameters of device.

The JV-curve obtained is shown in Figure III.18 (a). The solar cell parameters (Voc = 1.17 V, Jsc = 23.65 mA/cm^2 , FF = 87.46 % and PCE = 24.38 %) are obtained under optimum conditions in the simulation which is very promising result and further enhancement in this device is possible by optimizing the other parameters.

The quantum efficiency is very important parameters that expose the quality of the solar cell. The cell structure we have studied here has excellent quantum efficiency explained with Fig III.18 (b).

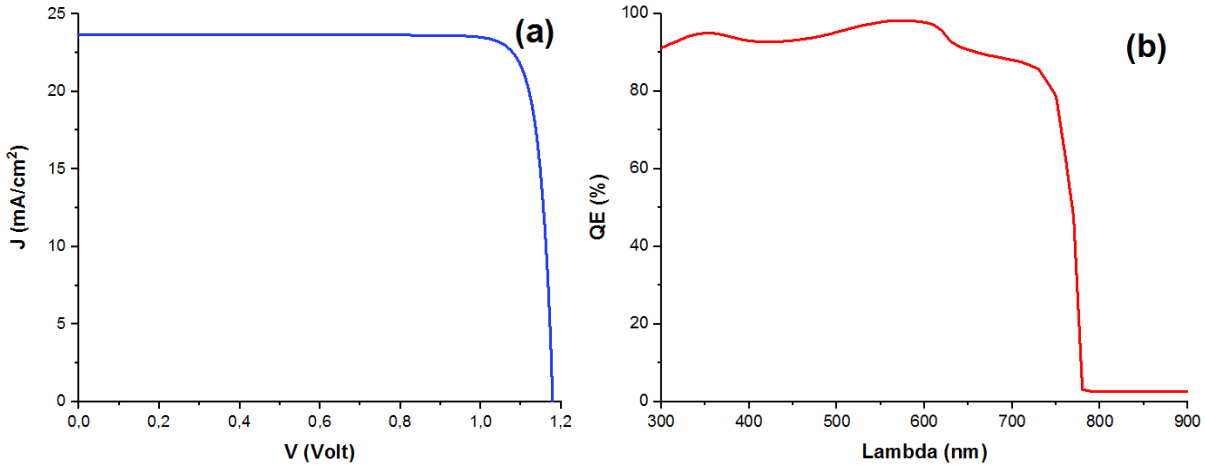

Fig III.18 J-V characteristics **(a)** and QE **(b)** of PSC with all optimum parameters.

Conclusion:

Perovskite solar cells have become a hot topic in the solar energy device area. With 10 years of development, the energy conversion efficiency has seen a great improvement from 3.9 % to more than 22%, and it still has great potential for further enhancement. Numerical simulation is a crucial technique in deeply understanding the operational mechanisms of solar cells and in predicting the maximum value of a solar cell with controlled design. This technique can also give guidance on the structure optimization for different devices.

In this simulation work, Glass FTO/TiO_2/$CH_3NH_3PbI_3$/Cu-based HTL/Au PSC device structure has been explored by using solar cell device simulator SCAPS-1D. comparing device performance with different HTM including CuSCN, CuI, CuO and Cu_2O , The effect of thickness and defect density of perovskite layer, defect at $CH_3NH_3PbI_3$/Cu_2O and TiO_2/$CH_3NH_3PbI_3$ interface, The effect of thickness and doping concentration of HTL layer (Cu_2O) as well as work function of back (Φm)contact were investigated. Our simulation concludes that: (1) Cu_2O as the best HTM among the HTL material proposed (2) the optimum thickness of absorber is 600nm (3) For achieving high photovoltaic performance the defect density in perovskite should be reduced up to $1x10^{14}$ cm^{-3} by improving the crystal structure and processing method (4) the $CH_3NH_3PbI_3$/Cu_2O interface defect has very less impact on device performance so the main attention should be paid to the interface defect created at TiO_2/$CH_3NH_3PbI_3$ interface during fabrication, thus to minimize the interface defect density at TiO_2/$CH_3NH_3PbI_3$ interface, appropriate interface passivation and modification is necessary and it should be kept less than or equal to 10^{10} cm^{-2} (5) the optimum thickness of HTL layer (Cu_2O) is 300nm (6) the doping concentration of Cu_2O (HTL) is $1x10^{19}$ cm^{-3} is sufficient to get desirable device performance (7) the selection of appropriate high work function back contact electrode (5eV) to get high built in voltage. The solar cell parameters (Voc = 1.17 V, Jsc = 23.65 mA/cm^2 , FF = 87.46 % and PCE = 24.38 %) are obtained under optimum conditions in the simulation which is very promising result and further enhancement in this device is possible by optimizing the other parameters. The simulation results obtained in this study would give a guide for practical fabrication process.

References:

[1] N.-Gyu. Park, Perovskite solar cells: an emerging photovoltaic technology, Materials Today, Vol 18, 66-72. (2015).

[2] O'Regan B, Gratzel M A low-cost, high-efficiency solar cell based on dye-sensitized colloidal TiO2 films. Nature 353(6346):737–740. (1991).

[3] Farzaneh et al, M.R.F, Bulk heterojunction polymer solar cell and perovskite solar cell: concepts, materials, current status, and opto-electronic properties. Sol. Energy 173, 407–424. (2018).

[4] Chen, C.-C et al. Perovskite/polymer monolithic hybrid tandem solar cells utilizing a low-temperature, full solution process. Mater. Horiz. 2 (2), 203–211.

[5] Kojima, A., Teshima, K., Shirai, Y., Miyasaka, T, Organometal halide perovskites as visible-light sensitizers for photovoltaic cells. J. Am. Chem. SOC.131, 6050–6051. (2009).

[6] Im, J.-H., Lee, C.-R., Lee, J.-W., Park, S.-W., Park, N.-G, 6.5% efficient perovskite quantum-dot-sensitized solar cell. Nanoscale 3 (10), 4088–4093. (2011).

[7] Kim HS et all. Lead iodide perovskite sensitized all-solid-state submicron thin film mesoscopic solar cell with efficiency exceeding 9%. Sci Rep, 2: 591. (2012).

[8] Lee, M et al. Efficient hybrid solar cells based on meso-super structured organometal halide perovskites. Science, 1228604. (2012).

[9] Malinkiewicz, O. et al. Perovskite solar cells employing organic charge- transport layers. Nature Photon. 8, 128–132. (2014).

[10] Burschka, J. et al. Sequential deposition as a route to high-performance perovskite sensitized solar cells. Nature 499, 316–319. (2013).

[11] Liu, M., Johnston, M. B., & Snaith, H. J. Efficient planar heterojunction perovskite solar cells by vapour deposition. Nature, 501(7467), 395. (2013).

[12] Green, M. A., Ho-Baillie, A., & Snaith, H. J. The emergence of perovskite solar cells. Nature Photonics, 8(7), (2014).

[13] Saliba, M et al. Cesium-containing triple cation perovskite solar cells: improved stability, reproducibility and high efficiency. Energy & Environmental Science, 9(6), 1989-1997. (2016).

[14] Yang, W. S et al. Iodide management in formamidinium-lead-halide–based perovskite layers for efficient solar cells. Science, 356(6345), 1376-1379. (2017).

[15] Simya OK, Mahaboobbatcha A, Balachander K. Compositional grading of CZTSSe alloy using exponential and uniform grading laws in SCAPS-ID simulation. Superlattices and Microstructures. Apr 1;92:285-93. (2016).

[16] Kieslich, G., Sun, S., Cheetham, A.K.: An extended tolerance factor approach for organic–inorganic perovskites. Chem. Sci. 6, 3430–3433. (2015).

[17] L. Hu et al Inverted Planar Perovskite Solar Cells with a High Fill Factor and Negligible Hysteresis by the Dual Effect of NaCl-Doped PEDOT:PSS. ACS Appl. Mater. Interfaces. 9(50), 43902–43909. (2017).

[18] N. Marinova, S. Valero, J.L. Delgado, J. Colloid Interface Sci. 488, 373. (2017).

[19] L. Etgar et al. Mesoscopic CH3NH3PbI3/Tio2 heterojunction solar cells. J. Am. Chem. Soc. 134, 17396– 17399. (2012).

[20] Q.Wang, Y. Xie, F. Soltani-Kordshuli, M. Eslamian, Renew. Sust. Energ. Rev. 56, 347. (2016).

[21] Snaith HJ, Abate A, Ball JM, Eperon GE, Leijtens T, Noel NK, et al. Anomalous hysteresis in perovskite solar cells. J Phys Chem Lett;5(9):1511–5. (2014).

[22] Ponseca Jr CS et al. Organometal halide perovskite solar cell materials rationalized ultrafast charge generation, high and microsecond-long balanced mobilities, and slow recombination. J Am Chem Soc;136(14):5189–92. (2014).

[23] Jung HS, Park NG. Perovskite solar cells from materials to devices. Small;11(1):10–25. (2015).

[24] P. P. Boix, K. Nonomura, N. Mathews and S. G. Mhaisalkar, Materials Today, 17, 16-23. (2014).

[25] K.Domanski, The Quest for Stability of Perovskite Solar Cells:Understanding Degradation, Improving Lifetimes and Towards Experimental Standards, thesis, federal institute of technology in Lausanne, (2018).

[26] Tress, W. et al. The role of the hole-transport layer in perovskite solar cells – reducing recombination and increasing absorption. 2014 40th photovolt. Spec. Conf. Pvsc1563-1566 (2014).

[27] Adhikari, N. et al. Interfacial Study To Suppress Charge Carrier Recombination for High Efficiency Perovskite Solar Cells. ACS Appl. Mater. Interfaces 7, 26445-26454. (2015).

[28] Istiak H et al. Functional materials, device architecture, and flexibility of perovskite solar cell. Emergent Materials 1:133–154. (2018)

[29] T. C. Sum & N. Mathews. Advancements in perovskite solar cells: photophysics behind the photovoltaics. Energy and Environmental Science, 7, 2518-2534. (2014).

[30] D. Bi et al. Polymer-templated nucleation and crystal groxth of perovskite films for solar cells with efficiency greater than 21%. Nature. 16142. (2016).

[31] J-H Im, J. Chung, S-J Kim & S-J Kim. Synthesis, structure, and photovoltaic property of a nanocrystalline 2H perovskite-type novel sensitizer (CH3CH2NH3)PbI3. Nanoscale Research Letters, volume 7. (2012).

[32] J-W Lee, D-J Seol, A-N Cho and N-G Park. High-Efficiency Perovskite Solar Cells Based on the Black Polymorph of HC(NH 2) 2 PbI 3. Advanced Materials, 26 (29), 4991-4998. (2014).

[33] D. Weber. CH3NH3PbX3, a Pb (II) -System with Cubic Perovskite Structure. Naturforsch, 33 (12), 1443-1445. (1978).

[34] Attfield JP, Lightfoot P. High-performance dye-sensitized solar cells based on solvent-free electrolytes produced from eutectic melts. , Morris RE Perovskites. Nat Mater 7(8):626–630. (2015).

[35] M.A. Loi, J.C. Hummelen, Hybrid solar cells: perovskites under the Sun. Nat. Mater. 12, 1087. (2013).

[36] L. Etgar et al. Mesoscopic CH3NH3PbI3/TiO2 heterojunction solar cells. J. Am. Chem. Soc. 134, 17396. (2012).

[37] N.J. Jeon et al. o-Methoxy substituents in spiro-OMeTAD for efficient inorganic-organic hybrid perovskite solar cells. J. Am. Chem. Soc. 136, 7837. (2014).

[38] J. Feng, B. Xiao, C. Structures, Optical properties, and effective mass tensors of CH3NH3PbX3 (X = I and Br) phases predicted from HSE06. J. Phys. Chem. Lett. 5, 1278. (2014).

[39] H. Zhou, Q. Chen, G. Li, S. Luo, T.B. Song, H.S. Duan, Z. Hong, J. You, Y. Liu, Y. Yang, Science 345 - 542. (2014).

[40] J.H. Noh, et al. Nano Lett. 13, 1764–1769. (2013)

[41] B. Conings, J. Drijkoningen, N. Gauquelin, A. Babayigit, J. D'Haen, Adv.Energy Mater., 5 - 15. (2015).

[42] N.J. Jeon, J.H. Noh, W.S. Yang, Y.C. Kim, S. Ryu, Nature, 517; 476-480. (2016).

[43] J.W. Lee, D.J. Seol, A.N. Cho, N.G. Park, Adv. Mater., 26, 4991-4998. (2014).

[44] F.C. Hanusch, E. Wiesenmayer, E. Mankel, A. Binek, P. Angloher, J. Phys. Chem. Lett., 5, 2791-5. (2014).

[45] Z. Li, M.J. Yang, J.S. Park, S.H. Wei, J.J. Berry, Chem. Mater., 28, 1. (2016).

[46] W.Hadouchi, study of the use of ZnO as an n-type contact in perovskite-based photovoltaic devices, university Paris Saclay, (2017).

[47] Kim, H.S et al. Lead iodide perovskite sensitized all-solid-state submicron thin film mesoscopic solar cell with efficiency exceeding 9 %. Sci.Rep. 2, 591, (2012).

[48] Y. Li, L. Meng, Y. Yang, G. Xu, Z. Hong, Q. Chen, J. You, G. Li, Y. Yang and Y. Li, Nat Commun, , 7. (2016).

[49] M. A. Green, K. Emery, Y. Hishikawa, W. Warta, E. D. Dunlop, D. H. Levi, A. W. Y. Ho-Baillie. Solar cell efficiency tables. Progress In Photovoltaics, 25 (1), 3-13. (2016).

[50] G. E. Eperon, V. M. Burlakov, P. Docampo, A. Goriely and H. J. Snaith, Advanced Functional

Materials, 24, 151-157. 2013.

[51] J.-W. Lee, H.-S. Kim, N.-G. Park. (2016), APbI3 (A = CH3NH3 and HC (NH2)2) Perovskite Solar Cells: From Sensitization to Planar Heterojunction, Organic-Inorganic Halide Perovskite Photovoltaics, Vol. 366, 223-253.

[52] A. Kojima, K. Teshima, Y. Shirai, T. Miyasaka, Organometal halide perovskites as visible-light sensitizers for photovoltaic cells. J.Am. Chem. Soc. 131, 6050–6051 (2009).

[53] H. Zhou, Q. Chen, G. Li, S. Luo, T. Song, H.-S. Duan, Z. Hong, J. You, Y. Liu, Y. Yang, Interface engineering of highly efficient perovskite solar cells. Science 345, 542–546 (2014).

[54] J. P. Correa Baena et al. Energy & Environmental Science, 2015, 8, 2928-2934.

[55] Q. Wali, A. Fakharuddin, I. Ahmed, M. H. Ab Rahim, J. Ismail and R. Jose, Journal of Materials Chemistry A, 2, 17427-17434. (2014).

[56] Z. Song, S.C. Watthage, A.B. Phillips, M.J. Heben, Pathways toward high-performance perovskite solar cells: review of recent advances in organo-metal halide perovskites for photovoltaic applications. J. Photonics Energy 6, 022001. (2016).

[57] H.-S. Kim, N.-G. Park, Parameters Affecting I–V Hysteresis of CH3NH3PbI3 Perovskite Solar Cells: Effects of Perovskite Crystal Size and Mesoporous TiO2 Laye. J. Phys. Chem. Lett.5(17), 2927–2934 (2014).

[58] H.-S. Kim, I.-H. Jang, N. Ahn,M. Choi, A. Guerrero, J. Bisquert,N.-G. Park, Control of I–V Hysteresis in CH3NH3PbI3 Perovskite Solar Cell. J. Phys. Chem. Lett. 6(22), 4633–4639. (2015).

[59] B. Chen, M. Yang, S. Priya, K. Zhu, Origin of J–V Hysteresis in Perovskite Solar Cells. J. Phys. Chem. Lett. 7(5), 905–917. (2016).

[60] M. Saliba et al. Incorporation of rubidium cations into perovskite solar cells improves photovoltaic performance. Science. 354(6309), 206–209 (2016).

[61] E.H. Anaraki et al. Highly efficient and stable planar perovskite solar cells by solution-processed tin oxide. Energy Environ. Sci. 9,3128–3134 (2016).

[62] J.-H. Im et al. 6.5% efficient perovskite quantum-dot-sensitized solar cell. Nanoscale 3, 4088–4093 (2011).

[63] Z. Shi, A.H. Jayatissa, Perovskites-Based Solar Cells: A Review of Recent Progress, Materials and Processing Methods.Materials.11(5), 729 (2018).

[64] V.M. Goldschmidt, Die Gesetze der Krystallochemie, Naturwissenschaften, 1926,14,477-485.

[65] Li, C., Soh, K. C. K., & Wu, P. Formability of ABO_3 perovskites. Journal of Alloys and Compounds, 372(1-2), 40-48. (2004).

[66] Noriko Onoda-Yamamur, Takasuke Matsuo, & Hiroshi suga. Calorimetric and IR Spectroscopic studies of transitions in methylammonium trihalogenoplumbates (II). J. Phy. Chem. Solids, 1383-1395. (1990).

[67] S.Pang et al. NH2CH=NH2PbI3 : An Alternative Organolead Iodide Perovskite Sensitizer for Mesoscopic Solar Cells. Chemistry of Materials, 26 (3), 1485–149. (2014).

[68] N.Ashurov et al. Mod. Electron. Mater., 3, 1–25. (2017).

[69] Li, C., Lu, X., Ding, W., Feng, L., Gao, Y., & Guo, Z. Formability of ABX_3 (X= F, Cl, Br, I) Halide Perovskites. Acta Crystallographic Section B: Structural Science, 64(6),702-707. (2008).

[70] R. Gottesman et al., "Photoinduced Reversible Structural Transformations in Free-Standing $CH_3NH_3PbI_3$ Perovskite Films," J. Phys. Chem. Lett., vol. 6, no. 12, pp. 2332–2338, Jun. (2015).

[71] L. Schmidt-Mende and J. Weickert, Organic and Hybrid Solar Cells: Walter de Gruyter GmbH, Berlin/Boston, (2016).

[72] Korshunova, K.; Winterfeld, L.; Beenken, W.J.D.; Runge, E. Thermodynamic stability of mixed Pb:Sn methyl-ammonium halide perovskites. Phys. Status Solidi 253, 1907–1915. (2016).

[73] J. Feng and B. Xiao, "Crystal Structures, Optical Properties, and Effective Mass Tensors of $CH_3NH_3PbX_3$ (X = I and Br) Phases Predicted from HSE06," J. Phys. Chem. Lett., vol. 5, no. 7, pp. 1278–1282, Apr. (2014).

[74] W.-J. Yin, J.-H. Yang, J. Kang, Y. Yan, and S.-H. Wei, "Halide Perovskite Materials for Solar Cells: a Theoretical Review," J. Mater. Chem. A, vol. 3, no. 17, pp. 8926–8942, (2015).

[75] Jixian XU, Materials interface engineering in perovskite photovoltaics, Thesis, Department of Electrical & Computer Engineering, University of Toronto (2017).

[76] H. S. Jung and N.-G. Park, "Perovskite Solar Cells: From Materials to Devices," Small, vol. 11 (1), pp. 10-25, (2015).

[77] Pankaj Yadav et al. " Exploring the performance limiting parameters of perovskite solar cell through experimental analysis and device simulation", Elsevier Journal of Solar Energy, Vol. 122, pp. 773-782, (2015).

[78] Q. Dong, Y. Fang, Y. Shao, P. Mulligan, J. Qiu, L. Cao and J. Huang, *Science*, **347**, 967-970. (2015).

[79] M. A. Green, A. Ho-Baillie and H. J. Snaith, *Nature Photonics*, 8, 506-514. (2014).

[80] E. J. Juarez-Perez, M. Wuβler, F. Fabregat-Santiago, K. Lakus-Wollny, E. Mankel, T.31 Mayer, W. Jaegermann and I. Mora-Sero, J. Phys. Chem. Lett., 5, 680–685. (2014).

[81] Gong-Ping Mao et al, Research progress in electron transport layer in perovskite solar cells, Rare Met. 37(2):95–106. (2018)

[82] G. Yang, H. Tao, P. Qin, W. Ke and G. Fang, J. Mater. Chem. A, 4, 3970–3990. (2016).

[83] Lin L, Jiang L, Qiu Y, Yu Y. Modeling and analysis of HTM-free perovskite solar cells based on ZnO electron transport layer. Superlattices Microstruct.104:167. (2017).

[84] Gheno.A et al. Printable WO3 electron transporting layer for perovskite solar cells: influence on device performance and stability. Sol Energy Mater Sol Cells. 161:347. (2017).

[85] Dong. QS et al. Insight into perovskite solar cells based on SnO2 compact electron-selective layer. J Phys Chem C. 119(19):10212. (2015).

[86] Wu CG, Chiang CH, Tseng ZL. Planar heterojunction perovskite/PC71BM solar cells with enhanced open-circuit voltage via (2/1)-step spin coating process. J Mater ChemA. 2014;2(38):15897.

[87] Jeng J, Chiang Y, Lee M, Peng S, Guo T. CH3NH3PbI3 perovskite/fullerene planar-heterojunction hybrid solar cells. Adv Mater. 25(27):3727. (2013).

[88] Yuli Xiong, Tongfa Liu, Xixi Jiang, Yaoguang Rong and Hongwei Han. Sci China Mater, 59(9): 757–768. (2016).

[89] S. Ito, Inorganic Hole-Transporting Materials for Perovskite Solar Cell, Springer International Publishing Switzerland (2016).

[90] Lee, M et al. Efficient Hybrid Solar Cells Based on Meso-Super structured Organometal Halide Perovskites. Science 338, 643–647 (2012).

[91] Habisreutinger, S. N. *et al.* Carbon Nanotube/Polymer Composites as a Highly Stable Hole Collection Layer in Perovskite Solar Cells. *Nano Lett.* **14,** 5561–5568 (2014).

[92] S.A Mhamed et al, Nanostructured materials for next generation energy storage and efficiency, pp 234.

[93] N.-G. Park et al, Inorganic Hole-Transporting Materials for Perovskite Solar Cell, Organic-Inorganic Halide Perovskite Photovoltaics, (2016).

[94] F.Azri et al, Electron and hole transport layers optimization by numerical simulation of a perovskite solar cell, Solar Energy 181, 372–378. (2019).

[95] Q. L. Wu et al. Kesterite Cu2ZnSnS4 as a Low Cost Inorganic Hole Transporting Material for High Efficiency Perovskite Solar Cells, ACS Applied Materials and Interfaces, 7 (2015).

[97] T. A. Berhe et al. "Organometal halide perovskite solar cells: degradation and stability," Energy & Environmental Science, vol. 9 (2), pp. 323-356, (2016).

[98] Takashi Minemoto, Masashi Murata, " Theoretical analysis on effect of band offsets in Perovskite solar cells", Elsevier Journal of Solar Energy Materials and Solar Cells, Vol. 133, pp. 8-14, February (2015).

[99] M.E, Recent Advances in Photovoltaic Technology based on Perovskite Solar Cell- A Review, International Research Journal of Engineering and Technology (IRJET) .Volume: 04 Issue: 07. July.(2017).

[100] Takashi Minemoto, Masashi Murata, " Impact of work function of back contact of perovskite solar cells without hole transport material analyzed by device simulation", Elsevier Journal of Current Applied Physics, Vol. 14, Issue 11, pp. 1428-1433, November (2014).

[101] Mohammad. I et al, " Copper Oxide as inorganic hole transport material for lead halide perovskite based solar cells", Elsevier Journal of Solar Energy, Vol. 120, pp. 370-380, October (2015).

[102] Buin, A. et al. Materials Processing Routes to Trap-Free Halide Perovskites. Nano Lett. (2014).

[103] Burgelman et al, SCAPS manual, no. May. (2014).

[104] Minemoto T, Murata M. Device modeling of perovskite solar cells based on structural similarity with thin film inorganic semiconductor solar cells. Journal of Applied Physics. 116: 5, 054505. (2014).

[105] Burgelman, M et al. Modeling thin-film PV devices. Progress in Photovoltaics: Research and Applications, 12(2-3), 143-153. (2004).

[106] J. A. Christians, R. C. M. Fung, P. V. Kamat, J. Am. Chem. Soc. 2014, 136, 758.

[107] Chaudhary, N.; Chaudhary, R.; Kesari, J. P.; Patra, A.; Chand, S. Copper Thiocyanate (CuSCN): An Efficient Solution-Processable Hole Transporting Layer in Organic Solar Cells. *J. Mater. Chem. C, 3* (45), 11886–11892. (2015).

[108] Amin.G ZnO and CuO nanostructures: low temperature growth, characterization, their optoelectronic and sensing applications *(1st ed. LiU-Tryck: Norrköping (Sweden))* [SE-60174]. (2012).

[109] B.A. Nejand, Cuprous oxide as a potential low cost hole transport material for stable perovskite solar cells. Chem sus Chem. 9(3),302-313 (2016).

[110] Wai-Yu Sit et al, High-Efficiency Fullerene Solar Cells Enabled by a Spontaneously Formed Mesostructured CuSCN-Nanowire Heterointerface. Adv. Sci. 5, 1700980. (2018).

[111] Paulina Sawicka-Chudy et al. J. Phys.: Conf. Ser. 1033 012002. (2018).

[112] M.N. Amalina, Photoconductivity of Copper (I) Iodide (CuI) Thin Films for Dye-Sensitized Solar Cells, ICECE (2010).

[113] Farhana Anwar, Effect of Different HTM Layers and Electrical Parameters on ZnO Nanorod-Based Lead-Free Perovskite Solar Cell for High-Efficiency Performance, International Journal of Photoenergy, ID 9846310, 9. (2017).

[114] B.S. Richards, "Single-material TiO2double-layer antireflection coatings,"Sol. Energy Mater. Sol. Cells, vol. 79, pp. 369−390, (2003).

[115] P. Löper et al,"Complex refractive index spectra of CH3NH3PbI3 perovskite thin films determined by spectroscopic ellipsometry and spectrophotometry,"J. Phys. Chem. Lett.vol. 6, pp. 66–71, Dec.(2014).